

## SYNTHESIS, CHARACTERIZATION, DFT, AND BIOLOGICAL ASSAY OF NEW XANTHATE COMPLEXES WITH NITROGEN BASES

Mohammed Mahmoud Molla-Babaker<sup>a\*</sup>, Maher Khalid<sup>a\*</sup>, Saad.E. AL-Mukhtar<sup>b\*</sup>

<sup>a</sup> Department of Chemistry, Faculty of Science, University of Zakho, Zakho, Kurdistan Region, Iraq.

<sup>b</sup> Department of Chemistry, College of science, University of Mosul, Iraq.

mohammed.babaker@uoz.edu.krd

maher.ali@uoz.edu.krd

Saadal\_Mukhtar@yahoo.com

Received: 10 Jan., 2023/ Accepted: 17 Mar., 2024 / Published: 23 May., 2024.

<https://doi.org/10.25271/sjuoz.2024.12.2.1250>

### ABSTRACT:

This study introduces a new series of complexes and adducts, denoted by  $[M(2-PhOEtXant)_2.nL]$ , where M represents Mn(II), Fe(II), Co(II), or Ni(II), and the ligand (2-PhOEtXant) is 2-Phenoxyethylxanthate. Varying ligands, including pyridine, piperidine, quinoline, ethylenediamine, and (1,10)-phenanthroline, are explored based on the value of n. Comprehensive characterization, encompassing techniques like <sup>1</sup>H-NMR, <sup>13</sup>C-NMR, FTIR, AA, CHN analysis, UV-visible spectroscopy, and magnetic property measurements, is employed. Results indicate an octahedral geometry for these complexes, as revealed by effective magnetic moment measurements and electronic spectra analysis. The compounds exhibit noteworthy antioxidant properties, demonstrated through the DPPH radical scavenging method, highlighting their potential as effective antioxidants. Moreover, the complexes display enhanced antibacterial activity against microbial strains compared to free ligands. This research not only delves into the coordination chemistry of these complexes but also underscores their diverse applications. Combining experimental methods with computational insights using Density Functional Theory (DFT) enhances the understanding of dithiolate transition metal complexes. The alignment of computational and experimental outcomes strengthens the reliability of the findings, laying a robust foundation for interdisciplinary exploration. The identified potential applications in optoelectronics, along with the notable antioxidant and antibacterial activities, position these complexes as promising contenders for advanced technologies and scientific applications.

**KEYWORD:** Complexes of [Manganese (II), Iron (II), Cobalt (II) & Nickel (II)], Xanthate Salt, Hexa-coordinate complexes and Xanthate complexes.

### 1. INTRODUCTION

Dithiolate transition metal complexes serve multiple critical functions, including their role as precursors for generating sulfide semiconductor materials and films. These complexes also excel at acting as stabilizers for nanoparticles and quantum dots. Moreover, they exhibit a wide range of properties, such as catalytic, antimicrobial, and antitumor activities (Mane et al., 2017) & (Al-Garah, 2017). Additionally, dithiolate complexes are extensively employed in the development of optical devices, photocells, and OLED devices. They are also utilized as photo-stabilizers and radiation protectors in polymers. Despite their widespread applications, there is still a need for a comprehensive investigation into the photochemistry and coordination compound behavior of dithiolate complexes in these contexts (Mikheylyis et al., 2023), (Gaikwad et al., 2020), (Solov'yev et al., 2019), (Jassim et al., 2021) & (Plyusnin et al., 2021).

In our ongoing research, we are actively engaged in synthesizing magnesium (II), iron (II), cobalt (II), and nickel (II) xanthates using both monodentate and bidentate N-donor ligands. Our primary objective is to advance our understanding of the coordination chemistry involving xanthate ligands. In this paper, we provide a comprehensive account detailing the procedures for synthesizing and characterizing adducts formed by nitrogen donor bases with the initial bis (2-phenoxyethylxanthato) metal (II) complex. The synthesis of these complexes involved the reaction of  $[M(PhOEtXant)_2]$  with the L ligand, utilizing molar ratios of either 1:1 or 1:2, in the presence of ethanol as the solvent. The specific type of L ligand,

\* Corresponding author

This is an open access under a CC BY-NC-SA 4.0 license (<https://creativecommons.org/licenses/by-nc-sa/4.0/>)

particularly the number of nitrogen donor atoms it contains, plays a crucial role in influencing the chelation process, ultimately leading to the binding of xanthate ligands to the central metal (II) atom.

Moreover, in this paper, we elaborate on the production and comprehensive analysis of the potassium 2-phenoxyethyl xanthate ligand and its corresponding metal compounds involving different divalent transition metal ions, such as Mn<sup>II</sup>, Fe<sup>II</sup>, Co<sup>II</sup>, and Ni<sup>II</sup>.

### 2. Experimental Section

#### A- Raw Materials and Solvents

All chemicals and solvents utilized in this study were of analytical grade. Carbon disulfide and 2-Phenoxyethanol were acquired from the Aldrich Company, while ethylenediamine, quinoline, (1,10)-Phenanthroline, and various metal chloride salts were sourced from the Alpha Company. Pyridine and piperidine were obtained from ROTH Company. Solvents, including ethanol, dimethylformamide (DMF), and diethyl ether, were procured from Scharlau Company.

#### B- Tools

For examining the synthesized ligands, a Bruker 500 MHz Ultrashield NMR spectrometer was employed to collect <sup>1</sup>H-NMR, <sup>13</sup>C-NMR, and Dept-135 spectra. Samples were dissolved in deuterated dimethylsulfoxide (DMSO) at room temperature (298 K), with tetramethylsilane (TMS) acting as the internal standard and measured at University of Tahrán, Iran. FT-IR spectra were recorded using a Perkin-Elmer 1710

spectrophotometer in the 350 to 4000  $\text{cm}^{-1}$  range, employing the KBr disc method. Electronic spectra were obtained in dimethylformamide (DMF) solvent with a concentration of  $10^{-3}$  M at 25°C using a Unicam HELIOS $\beta$  UV-VIS 2000 spectrophotometer instrument. Magnetic measurements were conducted at 25°C using the Gouy method in the solid state, utilizing a Sherwood scientific magnetic susceptibility balance. The melting points or decomposition temperatures of ligands and their complexes were determined using a Thermal Electro-Melting Point Apparatus 9300. Conductivity measurements for complexes were performed at a concentration of  $10^{-3}$  M in DMF solvent at 25°C, using an EC214 conductivity meter. Metal content was determined using atomic absorption spectroscopy (AA670 atomic absorption). These extensive analytical techniques collectively contributed to a detailed characterization of the synthesized ligands and their complexes, facilitating a comprehensive understanding of their structural, electronic, thermal, and chemical properties.

The synthesis process outlined involves the creation of a potassium 2-Phenoxyethyl xanthate ligand followed by the formation of various metal complexes. Below is a summary of the steps involved:

### Synthesis of Potassium 2-Phenoxy ethyl xanthate Ligand

The synthesis of the potassium 2-Phenoxy ethyl xanthate ligand involved the following steps:

First, 2.80 grams (0.05 moles) of potassium hydroxide were combined with 6.90 grams (0.05 moles) of 2-Phenoxyethanol, and the mixture was refluxed for one hour. Next, the mixture was cooled in an ice bath, and 3.80 grams (0.05 moles) of carbon disulfide were added drop-wise with continuous stirring over 30 minutes while still in the ice bath. The progress of the reaction was monitored using TLC (Thin Layer Chromatography) until it was complete (ethyl acetate and n-hexane 6:4). A yellow precipitate formed, which was then washed twice with 50 milliliters of diethyl ether. Afterwards, the precipitate was recrystallized with ethanol and subsequently dried under vacuum. This synthesis procedure is documented in the works (Al-fahdawi & Alsalihi, 2018) & (McNaughten et al., 2016).

## 3. SYNTHESIS OF COMPLEXES

### A. Synthesis of complex $[M(2\text{-Phenoxyethylxanthate})_2(L)_2]$

In this step, we synthesized the complex  $[M(2\text{-Phenoxyethylxanthate})_2(L)_2]$ , where L can be Pyridine, Piperidine, or Quinoline, and M represents Mn(II), Fe(II), Co(II), Ni(II), Cu(II), or Zn(II).

We began by slowly adding an ethanolic solution of either  $\text{MnCl}_2 \cdot 4\text{H}_2\text{O}$  (1.98g, 0.01mol),  $\text{FeCl}_2 \cdot 4\text{H}_2\text{O}$  (1.98g, 0.01mol),  $\text{CoCl}_2 \cdot 6\text{H}_2\text{O}$  (2.38g, 0.01mol), or  $\text{NiCl}_2 \cdot 4\text{H}_2\text{O}$  (2.38g, 0.01mol)

to an ethanolic solution of potassium 2-Phenoxyethylxanthate (5.04g, 0.02mol) while stirring. Subsequently, we introduced (0.02mol) of either pyridine, piperidine, or quinoline drop by drop, maintaining continuous stirring for 30 minutes. The resulting precipitate was separated through filtration, washed with ethanol, and then dried under vacuum.

### B. Synthesis of complex $[M(2\text{-Phenoxyethylxanthate})_2(L)]$

In this section, we prepared the complex  $[M(2\text{-Phenoxyethylxanthate})_2(L)]$ , where L can be either 1,10-Phenanthroline or Ethylenediamine.

The process involved slowly adding an ethanolic solution of  $\text{MnCl}_2 \cdot 4\text{H}_2\text{O}$  (1.98g, 0.01mol),  $\text{FeCl}_2 \cdot 4\text{H}_2\text{O}$  (1.98g, 0.01mol),  $\text{CoCl}_2 \cdot 6\text{H}_2\text{O}$  (2.38g, 0.01mol), or  $\text{NiCl}_2 \cdot 4\text{H}_2\text{O}$  (2.38g, 0.01mol) to an ethanolic solution of potassium 2-Phenoxyethylxanthate (5.04g, 0.02mol) while stirring. Next, (0.01mol) of either 1,10-phenanthroline or ethylenediamine was gradually added dropwise while maintaining continuous stirring for 30 minutes. The resulting precipitate was filtered, washed with ethanol, and then dried under vacuum.

## 4. DFT CALCULATION

The structure and characteristics of the synthesized complexes were analyzed through the application of the DFT technique. This analysis utilized the Dmol3 basis set in conjunction with the AGG approach. The computational investigation was carried out using the Material Studio program platform (Becke, n.d.), (Lee et al., 1988).

### Result and Discussion

The xanthate ligand was produced by reacting carbon disulfide with 2-phenoxyethanol in a basic medium using potassium hydroxide. Subsequently, the complexes were synthesized by directly combining  $\text{MnCl}_2 \cdot 4\text{H}_2\text{O}$ ,  $\text{FeCl}_2 \cdot 6\text{H}_2\text{O}$ ,  $\text{CoCl}_2 \cdot 6\text{H}_2\text{O}$ , or  $\text{NiCl}_2 \cdot 6\text{H}_2\text{O}$  with mixed ligands. These mixed ligands encompassed xanthate and nitrogen base adducts like Pyridine, Piperidine, Quinoline, 1,10-Phenanthroline, and Ethylenediamine, in molar ratios of either (1:2) or (1:1), as illustrated in (Fig. 1). To evaluate their properties, conductivity measurements of these prepared complexes were conducted in a dimethylformamide (DMF) solution, yielding reported conductivity values ranging from (4.6 - 44.6)  $\Omega^{-1} \cdot \text{cm}^2 \cdot \text{mol}^{-1}$ , indicating the absence of electrolytic behavior in the complexes. Table 1 provides a comprehensive summary of various physical characteristics associated with these synthesized compounds, encompassing melting points, color, metal content, and other pertinent attributes, offering a more profound understanding of the nature of these compounds.

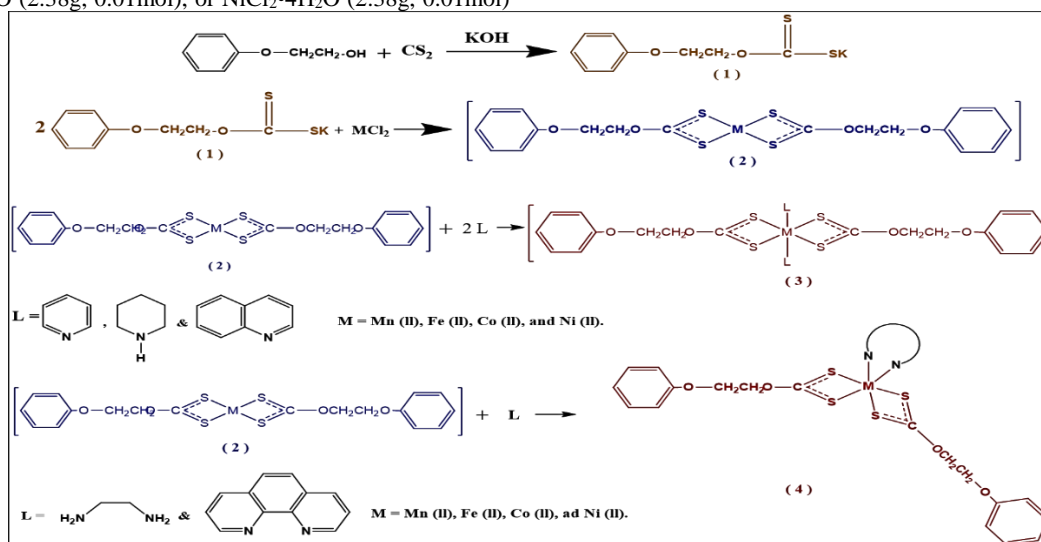


Figure 1: Synthesis of Potassium 2-Phenoxyethyl Xanthate Ligands and their Complexes

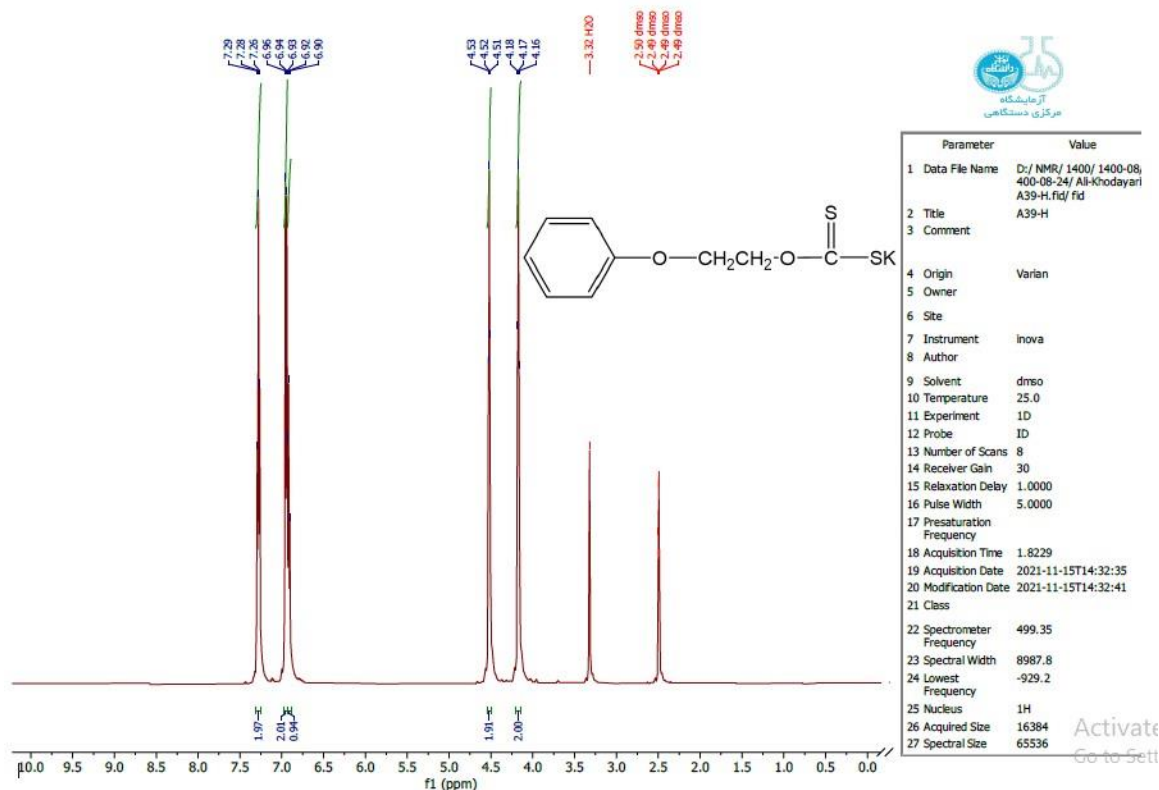
Table 1: Several of the produced compounds' physicochemical characteristics.

No.	Compounds	Colors	Molar conductivity $\Omega^{-1}.cm^2.mol^{-1}$	M% (Cal., Found)	Yield %
L	[(2-MeOEtXant) K]	Yellow	---	---	82.67
1.	[Mn(2-PhOEtXant) <sub>2</sub> (en)]	Grey	18.3	10.14 (9.95)	24.92
2.	[Mn(2-PhOEtXant) <sub>2</sub> (Phen)]	White	4.6	8.30 (8.10)	44.31
3.	[Mn(2-PhOEtXant) <sub>2</sub> (Py) <sub>2</sub> ]	Light Grey	11.3	8.59 (8.34)	69.21
4.	[Mn(2-PhOEtXant) <sub>2</sub> (Piper) <sub>2</sub> ]	Brown	8.2	8.45 (8.12)	42.51
5.	[Mn(2-PhOEtXant) <sub>2</sub> (Quino) <sub>2</sub> ]	Light Yellow	19.8	7.43 (7.13)	57.53
6.	[Fe(2-PhOEtXant) <sub>2</sub> (en)]	Grey	5.3	10.29 (10.22)	75.69
7.	[Fe(2-PhOEtXant) <sub>2</sub> (Phen)]	Brown	19.7	8.43 (8.25)	78.35
8.	[Fe(2-PhOEtXant) <sub>2</sub> (Py) <sub>2</sub> ]	Red	23.4	8.72 (8.48)	42.39
9.	[Fe(2-PhOEtXant) <sub>2</sub> (Piper) <sub>2</sub> ]	Red	18.8	8.58 (8.34)	51.16
10.	[Fe(2-PhOEtXant) <sub>2</sub> (Quino) <sub>2</sub> ]	Red-Brown	27.7	7.54 (7.34)	61.34
11.	[Co(2-PhOEtXant) <sub>2</sub> (en)]	Dark Brown	8.3	10.80 (10.56)	73.53
12.	[Co(2-PhOEtXant) <sub>2</sub> (Phen)]	Red-Brown	19.2	8.85 (8.49)	64.79
13.	[Co(2-PhOEtXant) <sub>2</sub> (Py) <sub>2</sub> ]	Green	26.3	9.16 (8.86)	64.05
14.	[Co(2-PhOEtXant) <sub>2</sub> (Piper) <sub>2</sub> ]	Dark Green	8.8	9.01 (8.56)	73.31
15.	[Co(2-PhOEtXant) <sub>2</sub> (Quino) <sub>2</sub> ]	Dark Green	44.6	7.92 (7.45)	82.61
16.	[Ni(2-PhOEtXant) <sub>2</sub> (en)]	Green	14.6	10.76 (10.70)	93.83
17.	[Ni(2-PhOEtXant) <sub>2</sub> (Phen)]	Brown	22.4	8.82 (8.68)	80.81
18.	[Ni(2-PhOEtXant) <sub>2</sub> (Py) <sub>2</sub> ]	Green	9.5	9.12 (8.99)	67.21
19.	[Ni(2-PhOEtXant) <sub>2</sub> (Piper) <sub>2</sub> ]	Yellow	14.2	8.98 (8.73)	96.23
20.	[Ni(2-PhOEtXant) <sub>2</sub> (Quino) <sub>2</sub> ]	Light Brown	36.2	7.89 (7.65)	51.34

### Nuclear Magnetic Resonance (NMR) Analysis

The ligand's structure was determined through NMR analysis using a 500 MHz instrument. The chemical shifts (<sup>1</sup>H-NMR-500MHz; Dimethylsulfoxide) in ppm for the ligand revealed specific values:  $\delta = 7.28$  (t, J=7.7 Hz, 2H, Ar-H),  $\delta = 6.93$  (dd, J=7.8 Hz, 3H, Ar-H),  $\delta = 4.52$  (t, J=4.9Hz, 2H, CH<sub>2</sub>), and  $\delta = 4.17$  (t, J=4.9 Hz, 2H, CH<sub>2</sub>), as depicted in (Figs. 2 and

3). Additionally, the <sup>13</sup>C NMR (101 MHz, Dimethylsulfoxide) exhibited chemical shifts at  $\delta$  66.42, 69.36, 114.80, 120.89, 121.00, 129.99, and 158.84, with the strong signal at 40 attributed to the Dimethylsulfoxide solvent. Further analysis using DEPT-135 indicated three positive signals for (CH-Ar) and two negative signals for 2(CH<sub>2</sub>). The disappearance signal at 158.84 in both positive and negative sides of DEPT-135 confirmed the presence of the thionyl (C=S) signal, as illustrated in (Figs. 4 and 5).

Figure 2: <sup>1</sup>H-NMR of K(2-PhOEtXant) Ligand.

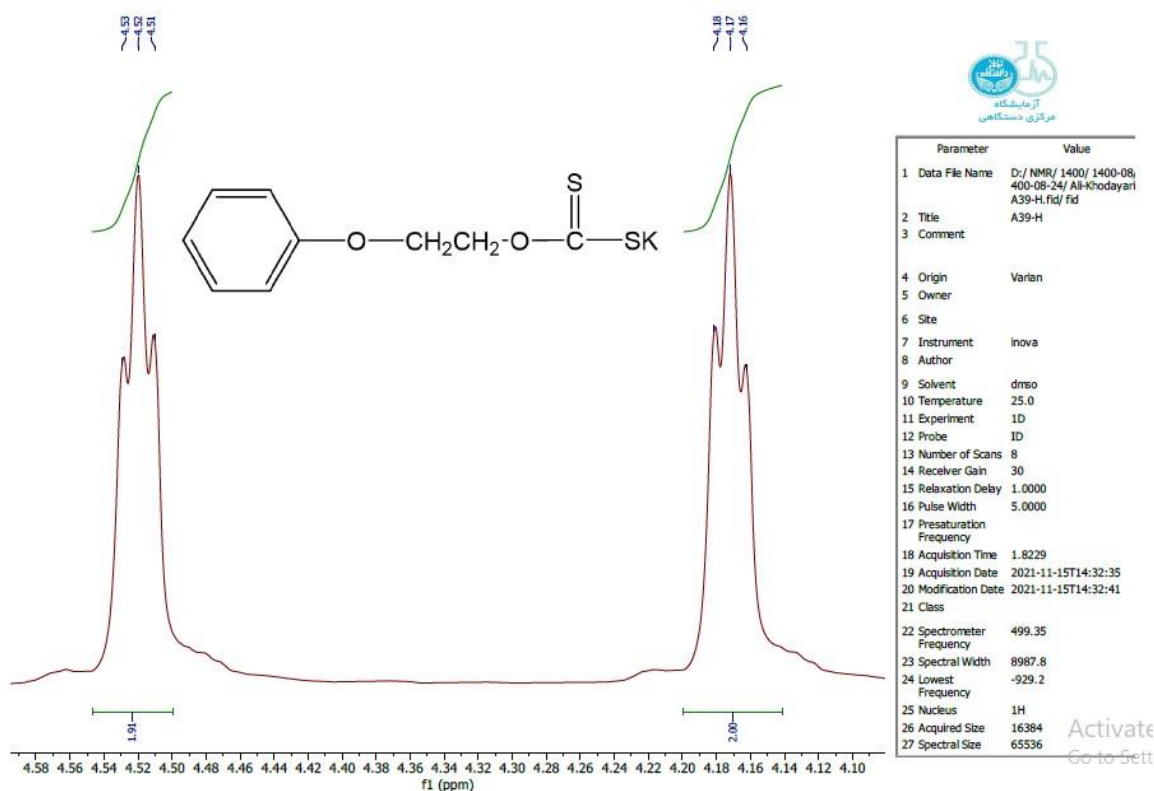


Figure 3: Expansion <sup>1</sup>H-NMR of K(2-PhOEtXant) Ligand.

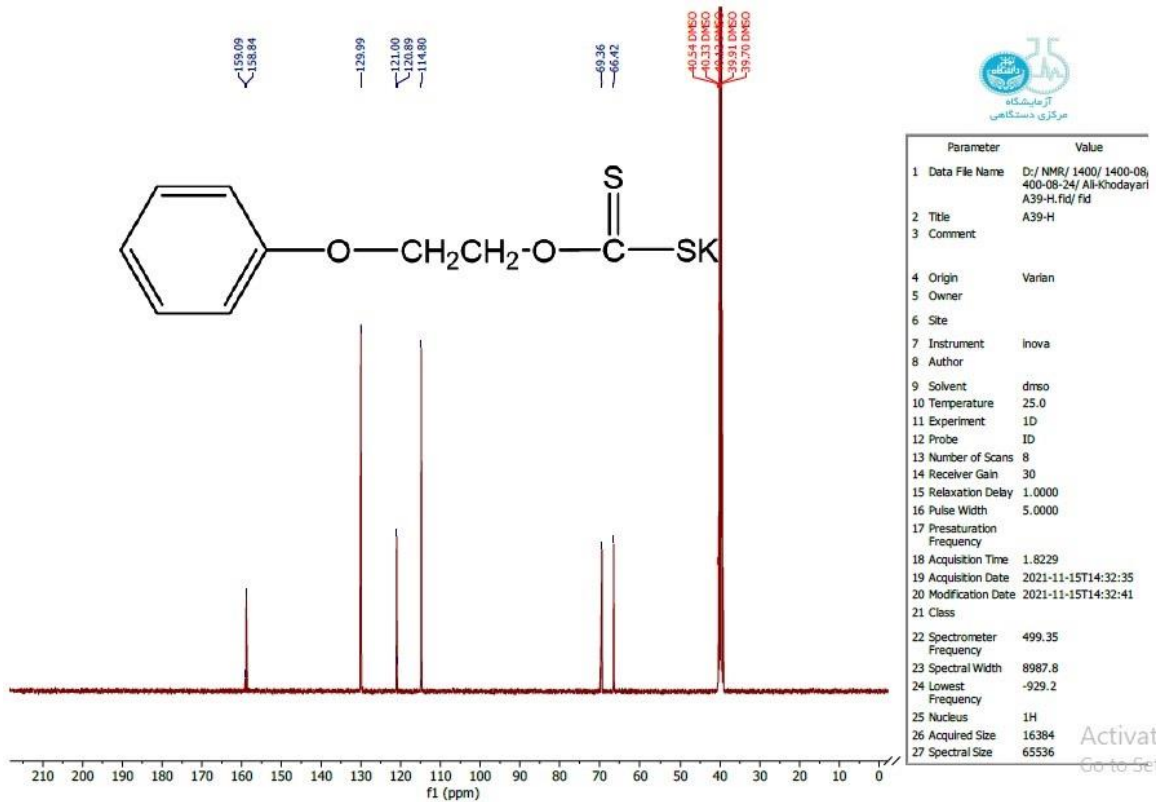
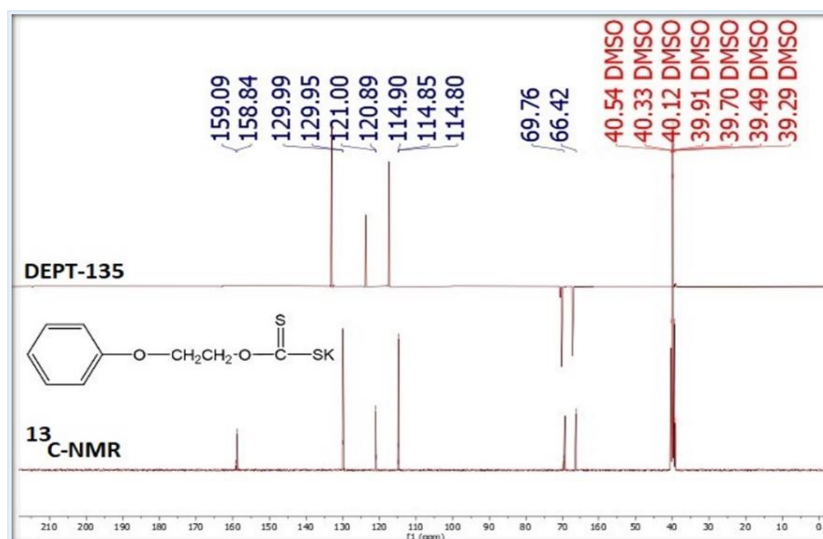


Figure 4: <sup>13</sup>C-NMR of K(2-PhOEtXant) Ligand.

Figure 5:  $^{13}\text{C}$ -NMR and DEPT-135 of K(2-PhOEtXant) Ligand.

### FTIR Investigations

The key IR bands of the ligand (2-PhOEtXant)K and its complexes are presented in (Table 2). The  $\nu(\text{C}-\text{O})$  band in the ligand spectrum, originally at  $1139\text{ cm}^{-1}$ , exhibited a shift to higher frequencies within the range of  $(1195\text{-}1252)\text{ cm}^{-1}$  in the complexes. Meanwhile, the  $\nu(\text{C}-\text{S})$  band at  $1095\text{ cm}^{-1}$  in the ligand shifted to lower frequencies  $(1002\text{-}1076)\text{ cm}^{-1}$  in the complexes. These shifts, both positive and negative, relative to the ligand, strongly suggest coordination of the xanthate ligand with the metal through the sulfur atoms, indicating symmetrical bidentate binding of the dithiocarbonate moiety (Heimbach et al., 2023), (Andotra et al., 2014) and (Khoo et al., 2014).

The IR spectra revealed a new band of medium to strong intensity in the  $(354\text{-}412)\text{ cm}^{-1}$  range, indicating  $\nu(\text{M}-\text{S})$  and

suggesting electron release from the alcohol, directing high electron density toward the sulfur atoms. The  $\nu(\text{M}-\text{N})$  was observed in the  $(455\text{-}513)\text{ cm}^{-1}$  zone (Vakalopoulou et al., 2020) & (Rathore et al., 2007). Another stretching frequency band at  $2933\text{ cm}^{-1}$ , attributed to C-H bonds in the ligand, shifted to the range  $(2924\text{ - }2987)\text{ cm}^{-1}$  in all complexes.

In the nitrogen bases, the  $\nu(\text{N}-\text{H})$  bands of ethylenediamine (en) and piperidine (piper) were observed at lower frequencies  $(3255\text{-}3498)\text{ cm}^{-1}$  (Montagner et al., 2011), supporting coordination with metal ions. Additionally, the  $\nu(\text{C}=\text{N})$  ring band appeared in the range of  $(1562\text{-}1647)\text{ cm}^{-1}$ , indicating coordination of the donor atoms with the metal ions (Rajput et al., 2012).

Table 2: FT-IR bands of the most important bonds of the ligand and their complexes

No.	Compounds	$\nu\text{ C-H}$ $\text{sp}^3$	$\nu\text{ C-H}$ $\text{sp}^2$	$\nu\text{ N-H}$	$\nu\text{ C}=\text{N}$	$\nu\text{ C-O}$	$\nu\text{ C-S}$	$\nu\text{ M-S}$	$\nu\text{ M-N}$
L	K (2-PhOEtXant)	2933	3043	---	---	1139	1095	---	---
1.	[Mn(2-PhOEtXant) <sub>2</sub> (en)]	2951	3030	3394	1600	1245	1076	389	455
2.	[Mn(2-PhOEtXant) <sub>2</sub> (O-Phen)]	2960	3055	---	1593	1242	1064	408	509
3.	[Mn(2-PhOEtXant) <sub>2</sub> (Py) <sub>2</sub> ]	2931	3039	---	1597	1222	1064	358	509
4.	[Mn(2-PhOEtXant) <sub>2</sub> (Piper) <sub>2</sub> ]	2935	3020	3414	1597	1246	1037	358	509
5.	[Mn(2-PhOEtXant) <sub>2</sub> (Quino) <sub>2</sub> ]	2951	3040	---	1600	1242	1037	362	479
6.	[Fe(2-PhOEtXant) <sub>2</sub> (en)]	2924	3036	---	1674	1252	1067	374	489
7.	[Fe(2-PhOEtXant) <sub>2</sub> (O-Phen)]	2939	3051	---	1562	1230	1018	381	424
8.	[Fe(2-PhOEtXant) <sub>2</sub> (Py) <sub>2</sub> ]	2951	3059	---	1597	1222	1037	362	509
9.	[Fe(2-PhOEtXant) <sub>2</sub> (Piper) <sub>2</sub> ]	2931	3010	3452	1604	1242	1014	385	489
10.	[Fe(2-PhOEtXant) <sub>2</sub> (Quino) <sub>2</sub> ]	2924	3025	---	1597	1242	1041	412	478
11.	[Co(2-PhOEtXant) <sub>2</sub> (en)]	2927	3012	3255	1589	1211	1014	366	505
12.	[Co(2-PhOEtXant) <sub>2</sub> (O-Phen)]	2927	3062	---	1597	1211	1014	378	509
13.	[Co(2-PhOEtXant) <sub>2</sub> (Py) <sub>2</sub> ]	2927	3075	---	1597	1211	1014	393	513
14.	[Co(2-PhOEtXant) <sub>2</sub> (Piper) <sub>2</sub> ]	2935	3059	3498	1597	1238	1002	385	505
15.	[Co(2-PhOEtXant) <sub>2</sub> (Quino) <sub>2</sub> ]	2927	3040	---	1597	1211	1056	374	509
16.	[Ni(2-PhOEtXant) <sub>2</sub> (en)]	2987	3050	---	1647	1238	1049	385	513

17.	[Ni(2-PhOEtXant) <sub>2</sub> (O-Phen)]	2927	3022	---	1589	1234	1049	389	509
18.	[Ni(2-PhOEtXant) <sub>2</sub> (Py) <sub>2</sub> ]	2958	3051	---	1597	1246	1026	374	513
19.	[Ni(2-PhOEtXant) <sub>2</sub> (Piper) <sub>2</sub> ]	2943	---	3414	1581	1238	1022	385	516
20.	[Ni(2-PhOEtXant) <sub>2</sub> (Quino) <sub>2</sub> ]	2978	3059	---	1585	1238	1049	381	509

### Magnetic Susceptibility Measurements

The complexes were analyzed for their effective magnetic moments ( $\mu_{eff}$ ) at a temperature of 25°C, and the outcomes are showcased in (Table 3). These magnetic moments, which span from 2.69 to 6.40, signify that the complexes possess an octahedral geometry. This finding corroborates with the theoretical spin-only magnetic moment value, as elucidated by (Al-Fahdawi & Alsalihi, 2018) and (Nicholls, 2013).

### Electronic Spectra Interpretation

The UV-Visible spectra were recorded for both the ligand and its complexes in a 10<sup>-3</sup> M DMF solution, and the findings are outlined in (Table 4). The absorption bands observed at the range (33783 and 31347 cm<sup>-1</sup>) in the spectra of complexes 1-5 are associated with charge transfer transitions. Because of the high spin d<sup>5</sup> manganese (II) configuration, which entails five unpaired electrons, the (d-d) electronic transitions are both spin-forbidden and Laporte-forbidden. Consequently, the absorption intensities within the conventional (d-d) absorption band are roughly 100 times lower, rendering the spectra not visible in the visible spectrum. The UV-Visible spectra of the Fe(II) complexes (6-10) displayed absorption bands in the range of (10917 – 11876) cm<sup>-1</sup>, corresponding to a transition of (<sup>5</sup>T<sub>2g</sub>→<sup>5</sup>E<sub>g</sub>). This strongly

suggests an octahedral geometry around the Fe(II) ions, consistent with findings from (Heimbach et al., 2023), (Batten & Robson, 1998) and (10917-11876).

For the Co(II) complexes (11-15), three absorption bands were observed spanning the ranges (10869-11415 cm<sup>-1</sup>), (15220-16286 cm<sup>-1</sup>), and (17393-21141 cm<sup>-1</sup>). These were identified as transitions from [<sup>4</sup>T<sub>1g</sub>(F)→<sup>4</sup>T<sub>1g</sub>(F)], (<sup>4</sup>T<sub>1g</sub>(F) → <sup>4</sup>A<sub>2g</sub>(F)), and (<sup>4</sup>T<sub>1g</sub>(F)→<sup>4</sup>T<sub>1g</sub>(P)], indicating an octahedral configuration for the Co(II) complexes, aligning with (Siddiqi & Nishat, 2000) and (Martell, 1971). Finally, the Ni(II) complexes (16-20) exhibited three absorption bands covering the ranges (10893-11655 cm<sup>-1</sup>), (15290-16103 cm<sup>-1</sup>), and (16920-21276 cm<sup>-1</sup>), corresponding to sequential transitions: [<sup>3</sup>A<sub>2g</sub>(F)→<sup>3</sup>T<sub>2g</sub>(F)], (<sup>3</sup>A<sub>2g</sub>(F)→<sup>3</sup>T<sub>1g</sub>(F)) and (<sup>3</sup>A<sub>2g</sub>(F)→<sup>3</sup>T<sub>1g</sub>(P)), as established by (AL-Mukhtar & AL-Jarah, 2019), (Shahzadi et al., 2009) and (Singh et al., 1989).

In all these compounds, a prominent high-intensity absorption peak was observed in the range of (35211-49504 cm<sup>-1</sup>), indicating  $\pi$  to  $\pi^*$  and  $n$  to  $\pi^*$  intra-ligand transitions. Additionally, a lower-intensity band in the near UV region, spanning (25493-36101 cm<sup>-1</sup>), was attributed to ligand to metal charge transfer bands (LMCT) transitions, as suggested by (Griffith et al., 2011). This summary encapsulates the UV-Visible spectra data, highlighting the associated transitions and geometries for the mentioned complexes and their ligand.

Table 3: presents the effective magnetic moment values and electronic spectral data for both the ligand and the prepared complexes.

NO	Compounds	U-Vis. bands (cm <sup>-1</sup> )	Assignment	$\mu_{eff} B. M$	Proposed Structure
L	K (2-PhOEtXant)	46728, 42372, 39682, 35211	$\pi \rightarrow \pi^*, n \rightarrow \pi^*$	----	----
1.	[Mn(2-PhOEtXant) <sub>2</sub> (en) <sub>2</sub> ]	49019, 45248, 38461 33670, 32362	$\pi \rightarrow \pi^*, n \rightarrow \pi^*$ C.T	6.37	Octahedral
2.	[Mn(2-PhOEtXant) <sub>2</sub> (Phen) <sub>2</sub> ]	49019, 44052, 38910 33783, 31347	$\pi \rightarrow \pi^*, n \rightarrow \pi^*$ C.T	6.12	Octahedral
3.	[Mn(2-PhOEtXant) <sub>2</sub> (Py) <sub>2</sub> ]	49504, 44052, 40485 33670, 31446	$\pi \rightarrow \pi^*, n \rightarrow \pi^*$ C.T	6.14	Octahedral
4.	[Mn(2-PhOEtXant) <sub>2</sub> (Piper)]	49261, 47393, 44052, 40650 33783, 32573, 31446	$\pi \rightarrow \pi^*, n \rightarrow \pi^*$ C.T	6.20	Octahedral
5.	[Mn(2-PhOEtXant) <sub>2</sub> (Quino)]	49504, 47619, 40000 36101, 33783, 31446	$\pi \rightarrow \pi^*, n \rightarrow \pi^*$ C.T	6.06	Octahedral
6.	[Fe(2-PhOEtXant) <sub>2</sub> (en) <sub>2</sub> ]	48543, 43103, 40650 34364, 33898, 31446 10940	$\pi \rightarrow \pi^*, n \rightarrow \pi^*$ C.T ( <sup>5</sup> T <sub>2g</sub> → <sup>5</sup> E <sub>g</sub> )	4.71	Octahedral
7.	[Fe(2-PhOEtXant) <sub>2</sub> (Phen) <sub>2</sub> ]	46082, 42918, 38461 32154, 31446, 25493 10917	$\pi \rightarrow \pi^*, n \rightarrow \pi^*$ C.T ( <sup>5</sup> T <sub>2g</sub> → <sup>5</sup> E <sub>g</sub> )	4.82	Octahedral
8.	[Fe(2-PhOEtXant) <sub>2</sub> (Py) <sub>2</sub> ]	47619, 43859, 39525 33783, 32786, 31446 10952	$\pi \rightarrow \pi^*, n \rightarrow \pi^*$ C.T ( <sup>5</sup> T <sub>2g</sub> → <sup>5</sup> E <sub>g</sub> )	5.29	Octahedral
9.	[Fe(2-PhOEtXant) <sub>2</sub> (Piper)]	48780, 44052, 39215 33783, 32573, 31446 10928	$\pi \rightarrow \pi^*, n \rightarrow \pi^*$ C.T ( <sup>5</sup> T <sub>2g</sub> → <sup>5</sup> E <sub>g</sub> )	4.84	Octahedral

10.	[Fe(2-PhOEtXant) <sub>2</sub> (Quino)]	47619, 45454, 38461	$\pi \rightarrow \pi^*, n \rightarrow \pi^*$	4.80	Octahedral
		34965, 32573, 31446	C.T		
		11876	( <sup>5</sup> T <sub>2g</sub> → <sup>5</sup> E <sub>g</sub> )		
11.	[Co(2-PhOEtXant) <sub>2</sub> (en) <sub>2</sub> ]	49261, 42918, 39370	$\pi \rightarrow \pi^*, n \rightarrow \pi^*$	3.73	Octahedral
		34843, 33783, 28248	C.T		
		21141, 16103, 11415	( <sup>4</sup> T <sub>1g</sub> (F)→ <sup>4</sup> T <sub>1g</sub> (F)) , ( <sup>4</sup> T <sub>1g</sub> (F) → <sup>4</sup> A <sub>2g</sub> (F)) &( <sup>4</sup> T <sub>1g</sub> (F)→ <sup>4</sup> T <sub>1g</sub> (P) )		
12.	[Co(2-PhOEtXant) <sub>2</sub> (Phen) <sub>2</sub> ]	45248, 39682, 38314	$\pi \rightarrow \pi^*, n \rightarrow \pi^*$	3.90	Octahedral
		33783, 31347, 27322	C.T		
		20576, 16286, 10905	( <sup>4</sup> T <sub>1g</sub> (F)→ <sup>4</sup> T <sub>1g</sub> (F)) , ( <sup>4</sup> T <sub>1g</sub> (F) → <sup>4</sup> A <sub>2g</sub> (F)) & ( <sup>4</sup> T <sub>1g</sub> (F)→ <sup>4</sup> T <sub>1g</sub> (P))		
13.	[Co(2-PhOEtXant) <sub>2</sub> (Py) <sub>2</sub> ]	44052, 40650, 38461, 35211	$\pi \rightarrow \pi^*, n \rightarrow \pi^*$	3.94	Octahedral
		31446, 29325, 27472	C.T		
		21097, 16103, 10869	( <sup>4</sup> T <sub>1g</sub> (F)→ <sup>4</sup> T <sub>1g</sub> (F)) , ( <sup>4</sup> T <sub>1g</sub> (F) → <sup>4</sup> A <sub>2g</sub> (F)) & ( <sup>4</sup> T <sub>1g</sub> (F)→ <sup>4</sup> T <sub>1g</sub> (P))		
14.	[Co(2-PhOEtXant) <sub>2</sub> (Piper)]	44052, 40650, 37174	$\pi \rightarrow \pi^*, n \rightarrow \pi^*$	3.96	Octahedral
		34129, 31250, 30120, 27322	C.T		
		17393, 15220, 10893	( <sup>4</sup> T <sub>1g</sub> (F)→ <sup>4</sup> T <sub>1g</sub> (F)) , ( <sup>4</sup> T <sub>1g</sub> (F) → <sup>4</sup> A <sub>2g</sub> (F)) & ( <sup>4</sup> T <sub>1g</sub> (F)→ <sup>4</sup> T <sub>1g</sub> (P))		
15.	[Co(2-PhOEtXant) <sub>2</sub> (Quino)]	44052, 39525, 38314	$\pi \rightarrow \pi^*, n \rightarrow \pi^*$	4.23	Octahedral
		31347, 29850, 28735, 27397	C.T		
		20964, 16077, 10881	( <sup>4</sup> T <sub>1g</sub> (F)→ <sup>4</sup> T <sub>1g</sub> (F)) , ( <sup>4</sup> T <sub>1g</sub> (F) → <sup>4</sup> A <sub>2g</sub> (F)) & ( <sup>4</sup> T <sub>1g</sub> (F)→ <sup>4</sup> T <sub>1g</sub> (P))		
16.	[Ni(2-PhOEtXant) <sub>2</sub> (en) <sub>2</sub> ]	44642, 40160, 36900	$\pi \rightarrow \pi^*, n \rightarrow \pi^*$	2.97	Octahedral
		30769, 29239, 26455	C.T		
		21276, 15290, 11198	( <sup>3</sup> A <sub>2g</sub> (F)→ <sup>3</sup> T <sub>2g</sub> (F)), ( <sup>3</sup> A <sub>2g</sub> (F)→ <sup>3</sup> T <sub>1g</sub> (F)) & ( <sup>3</sup> A <sub>2g</sub> (F)→ <sup>3</sup> T <sub>1g</sub> (P))		
17.	[Ni(2-PhOEtXant) <sub>2</sub> (Phen) <sub>2</sub> ]	47393, 42553, 36900	$\pi \rightarrow \pi^*, n \rightarrow \pi^*$	2.73	Octahedral
		31446, 29411, 26246	C.T		
		21052, 15873, 109643	( <sup>3</sup> A <sub>2g</sub> (F)→ <sup>3</sup> T <sub>2g</sub> (F)), ( <sup>3</sup> A <sub>2g</sub> (F)→ <sup>3</sup> T <sub>1g</sub> (F)) & ( <sup>3</sup> A <sub>2g</sub> (F)→ <sup>3</sup> T <sub>1g</sub> (P))		
18.	[Ni(2-PhOEtXant) <sub>2</sub> (Py) <sub>2</sub> ]	46296, 43478, 39682, 36630	$\pi \rightarrow \pi^*, n \rightarrow \pi^*$	2.81	Octahedral
		31347, 30030, 28818	C.T		
		16920, 15313, 10893	( <sup>3</sup> A <sub>2g</sub> (F)→ <sup>3</sup> T <sub>2g</sub> (F)), ( <sup>3</sup> A <sub>2g</sub> (F)→ <sup>3</sup> T <sub>1g</sub> (F)) & ( <sup>3</sup> A <sub>2g</sub> (F)→ <sup>3</sup> T <sub>1g</sub> (P))		
19.	[Ni(2-PhOEtXant) <sub>2</sub> (Piper)]	43290, 39840, 35460	$\pi \rightarrow \pi^*, n \rightarrow \pi^*$	2.69	Octahedral
		29850, 28818, 26178	C.T		
		17391, 16103, 11655	d - d		
20.	[Ni(2-PhOEtXant) <sub>2</sub> (Quino)]	45871, 41841, 39682, 36101	$\pi \rightarrow \pi^*, n \rightarrow \pi^*$	2.77	Octahedral
		31446, 30030, 28169	C.T		

	21052, 15313, 11185	( <sup>3</sup> A <sub>2</sub> g(F)→ <sup>3</sup> T <sub>2</sub> g(F)), ( <sup>3</sup> A <sub>2</sub> g(F)→ <sup>3</sup> T <sub>1</sub> g (F)) & ( <sup>3</sup> A <sub>2</sub> g(F)→ <sup>3</sup> T <sub>1</sub> g(P))	
--	---------------------	--	--

**Thermogravimetric Analysis TGA, DSC & DTA**

The thermal degradation of metal xanthate complexes was examined using TGA, DSC, and DTA techniques. TGA was conducted in the temperature range of room temperature to 800 °C. The TGA plot presented in (Fig. 6) reveals a substantial weight loss of 75%, occurring in a temperature range starting from 143 °C and continuing until 760 °C through three distinct steps, as illustrated in (Fig.7). This weight loss is attributed to the thermal decomposition of the xanthate complex [Ni(2-PhOEtXant)<sub>2</sub>(en)] into [NiS<sub>2</sub>], resulting in the formation of iron

sulfide and volatile compounds as end products (Cordova et al., 2021), (Faroughi Niya et al., 2021) and (Palaty et al., 2010). In Figure 4.55, DTA curves recorded for 4.2780 mg of [Ni(2-PhOEtXant)<sub>2</sub>(en)] powder reveal a distinct sharp endothermic peak around 143 °C, corresponding to the decomposition of [Ni(2-PhOEtXant)<sub>2</sub>(en)] into [NiS<sub>2</sub>]. The enthalpy changes (ΔH) value associated with this process is 28.79 J/g and specific heat capacity C<sub>p</sub> 0.008535 °C.min/mg. Some exothermic peaks observed in the figure indicate concurrent oxidation reactions during decomposition.

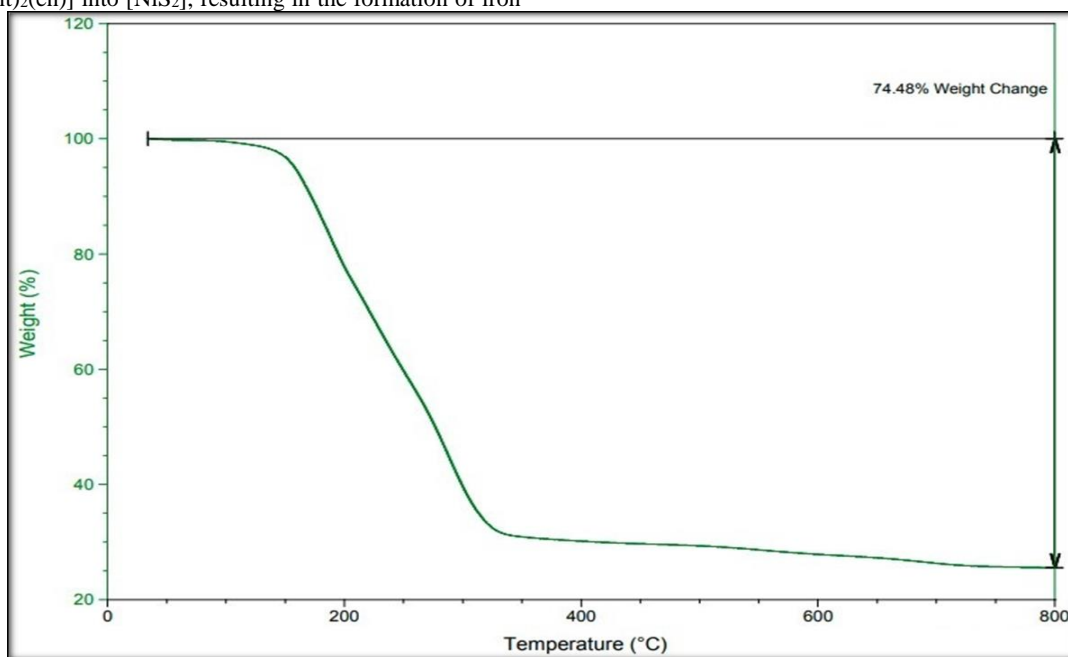


Figure 6: Thermo gravimetric analysis (TGA) profiles for [Ni(2-PhOEtXant)<sub>2</sub>(en)].

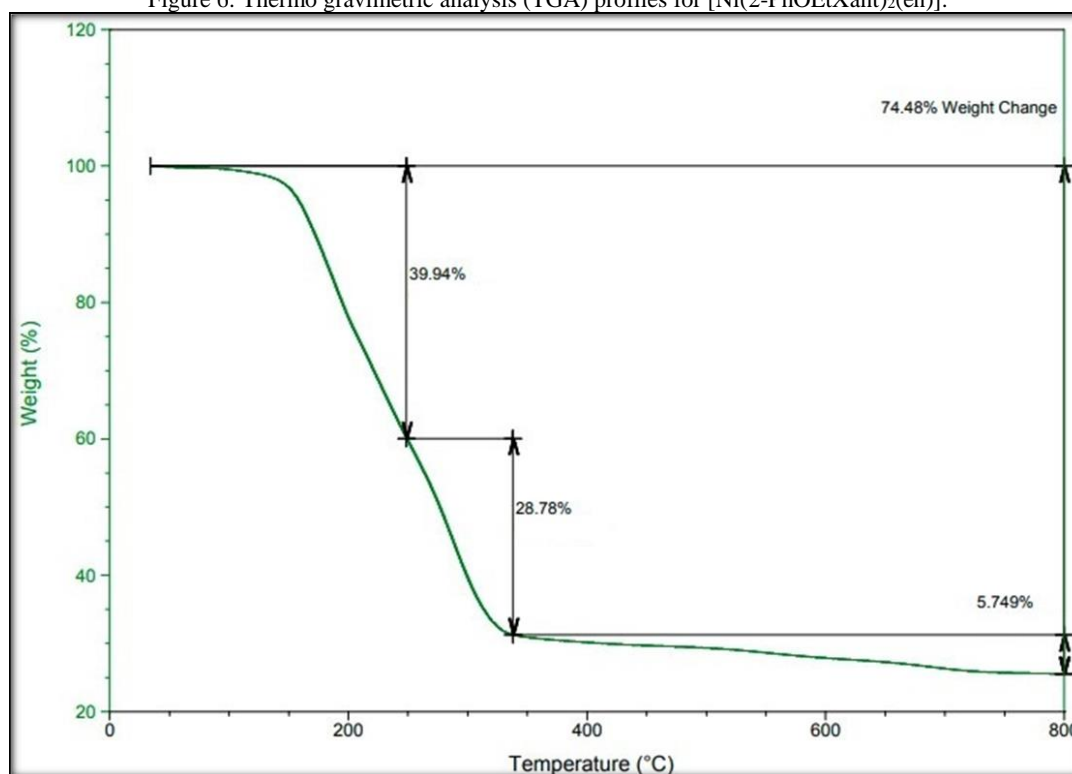


Figure 7: (TGA) Curve of [Zn(2-PhOEtXant)<sub>2</sub>(en)] within 3 Steps.

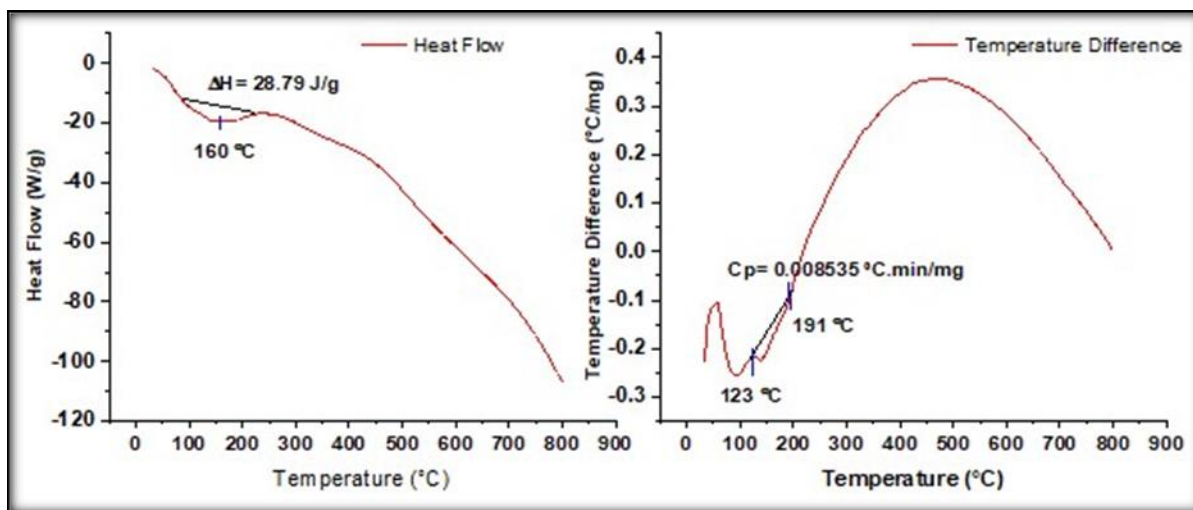


Figure 8: DSC & DTA Graph of [Zn(2-PhOEtXant)<sub>2</sub>(en)].

## 5. BIOLOGICAL ACTIVITY

### 1. Antioxidant Activity

This represents the most straightforward and widely utilized approach for assessing the antioxidant capabilities of both food items and numerous medicinal plant substances, as highlighted in studies by (Parcheta et al., 2021) and (Peyrat-Maillard et al., 2000). The evaluation of antioxidant activity in this method relies on the utilization of DPPH as a free radical. To perform this analysis, the xanthate ligand and its corresponding hexa-coordinate complexes are first dissolved in a minimal amount of DMSO and subsequently diluted with methanol to attain a concentration of 200 µg/ml. These initial stock solutions are further diluted to 20, 40, and 60 µg/ml. Each of these diluted solutions is then combined with 0.5 ml of freshly prepared methanolic solution containing 2,2-diphenyl-1-picrylhydrazyl at a concentration of 0.5 mM. The resulting mixture is left to incubate in a dark environment for a duration of 30 minutes at room temperature.

During this incubation period, the tested compounds interact with the DPPH radical, causing it to undergo reduction. This

reduction is indicated by a noticeable change in color from a deep violet hue to a lighter shade of yellow. The efficiency of scavenging DPPH radicals is subsequently assessed by measuring the absorbance of the mixture at a wavelength of 517 nm. To distinguish between the tested compounds and act as a reference, the absorbance of the DPPH radical without any antioxidant (control) and that of the reference compound (ascorbic acid) are also measured at the same concentrations. The percentage of inhibition (IP) of the DPPH radical is then calculated using the following equation, (Al Zoubi et al., 2017) and (Sreeju et al., 2016):

$$IP = \frac{A_c - A_s}{A_c} \times 100$$

Where

$A_c$  = Absorbance of the DPPH radical in methanol

$A_s$  = Absorbance of the DPPH + sample (tested sample/standard)

The average DPPH scavenging percentage (IP) of the compounds, tested in triplicate at various concentrations, the mean inhibition percentage at different concentrations, IC<sub>50</sub> value are provided in (Table 4).

Table 4: Antioxidant Function of the compounds.

No.	Concentration (µg/ml)	20	40	60	Mean of IP at varies conc.	IC <sub>50</sub>
	Compounds	Mean of IP (DPPH scavenging %)				
1.	(2-PhOEtXant) K	68.07	80.53	88.96	79.18	63.88
2.	[Mn(2-PhOEtXant) <sub>2</sub> (en)]	38.52	48.15	52.94	46.53	37.85
3.	[Mn(2-PhOEtXant) <sub>2</sub> (Phen)]	53.73	53.23	57.75	54.90	67.97
4.	[Mn(2-PhOEtXant) <sub>2</sub> (Py) <sub>2</sub> ]	56.77	59.52	61.33	59.20	38.68
5.	[Mn(2-PhOEtXant) <sub>2</sub> (Piper) <sub>2</sub> ]	54.37	55.96	60.76	57.03	44.07
6.	[Mn(2-PhOEtXant) <sub>2</sub> (Quino) <sub>2</sub> ]	49.25	54.22	60.64	54.70	40.89
7.	[Fe(2-PhOEtXant) <sub>2</sub> (en)]	32.66	38.74	41.15	37.51	37.15
8.	[Fe(2-PhOEtXant) <sub>2</sub> (Phen)]	32.66	34.28	61.79	42.91	52.39
9.	[Fe(2-PhOEtXant) <sub>2</sub> (Py) <sub>2</sub> ]	56.56	58.00	50.43	54.99	65.89
10.	[Fe(2-PhOEtXant) <sub>2</sub> (Piper) <sub>2</sub> ]	45.80	48.20	53.77	39.25	43.14
11.	[Fe(2-PhOEtXant) <sub>2</sub> (Quino) <sub>2</sub> ]	31.00	48.48	53.06	44.45	35.95
12.	[Co(2-PhOEtXant) <sub>2</sub> (en)]	82.26	89.01	88.98	86.75	19.10
13.	[Co(2-PhOEtXant) <sub>2</sub> (Phen)]	87.68	92.96	92.64	91.09	39.74
14.	[Co(2-PhOEtXant) <sub>2</sub> (Py) <sub>2</sub> ]	94.96	95.30	95.61	95.29	43.81
15.	[Co(2-PhOEtXant) <sub>2</sub> (Piper) <sub>2</sub> ]	87.33	89.10	94.26	91.09	37.68
16.	[Co(2-PhOEtXant) <sub>2</sub> (Quino) <sub>2</sub> ]	88.25	88.84	89.12	88.73	36.61
17.	[Ni(2-PhOEtXant) <sub>2</sub> (en)]	84.35	90.66	92.75	89.25	39.68
18.	[Ni(2-PhOEtXant) <sub>2</sub> (Phen)]	87.92	90.99	93.74	90.88	37.66
19.	[Ni(2-PhOEtXant) <sub>2</sub> (Py) <sub>2</sub> ]	84.36	91.50	94.90	90.25	38.08
20.	[Ni(2-PhOEtXant) <sub>2</sub> (Piper) <sub>2</sub> ]	77.71	80.46	81.95	80.04	38.76
21.	Ascorbic acid	93.05	93.54	93.88	93.49	39.16

The efficacy is measured by the inhibitory concentration IC<sub>50</sub>, indicating the quantity of antioxidants needed to reduce the initial DPPH• concentration by 50%. A lower IC<sub>50</sub> signifies increased "antiradical efficiency." The results of radical scavenging activity for all compounds are summarized in Table 4. Compound (12) displayed the best radical scavenging activity, with a value of (19.10) µg/ml, surpassing other compounds in comparison to ascorbic acid, which had a value of (39.16) µg/ml. Additionally, several other complexes (2, 4, 7, 11, 15, 16, 18, 19 & 20) exhibited notable activity with values ranging from (35.95) µg/ml to (38.76) µg/ml, again when compared to ascorbic acid (39.16) µg/ml (Ajiboye & Onwudiwe, 2022) and (Andotra et al., 2017).

## 2. Antibacterial Assay

The antibacterial activities of both xanthate ligands and their metal complexes were examined against a range of bacteria, including gram-positive (*Staphylococcus aureus*) and gram-negative (*Escherichia coli*). The screening was conducted using the agar disc diffusion method, which assesses antimicrobial activity by measuring the inhibition zone against the tested microorganisms. This approach provides valuable insights into the potential effectiveness of the studied compounds against both

types of bacteria. These bacteria were selected because they are recognized as common human pathogens (DHAKA & Choudhary, 2015). The assessment of activity was based on measuring the diameter of inhibitory zones (mm). In the evaluation of antibacterial activity between xanthate ligands and complexes, the xanthate ligands exhibit moderate to poor antibacterial activity. In contrast, the complexes demonstrate significantly improved antibacterial activity against microbial strains compared to the free ligands. This observed behavior can be attributed to the chelation effect, wherein the charge of the metal ion is reduced through neutralization with the sulfur charge present in the xanthate. Furthermore, chelation leads to increased liposolubility in complexes, facilitating enhanced permeation of the bacterial cell membrane as illustrated in (Table 5).

The antibacterial activity results indicate that the complexes [Co(L)<sub>2</sub>(Phen)] and [Fe(L)<sub>2</sub>(Py)<sub>2</sub>] exhibit higher antibacterial activity compared to the other complexes as represent in (Figs. 9 & 10). The extremely diluted 25% concentration of the stock solution demonstrates limited or negative activity in the majority of the complexes. These discoveries significantly contribute to our comprehension of the structure-activity relationship, shedding light on the potential applications of xanthate complexes as effective antibacterial agents.

Table 5: Bacterial activity of the xanthate ligands with some metals complexes.

No.	Compounds	Conc.	<i>Staphylococcus aureus</i>	<i>Escherichia coli</i>
L	K (2-PhOEtXant)	Stock	11mm	15mm
		75%	-	14mm
		50%	-	13mm
		25%	-	10mm
1.	[Fe(L) <sub>2</sub> (Py) <sub>2</sub> ]	Stock	15mm	20mm
		75%	14mm	18mm
		50%	13mm	15mm
		25%	12mm	14mm
2.	[Co(L) <sub>2</sub> (Phen)]	Stock	18mm	25mm
		75%	13mm	15mm
		50%	12mm	-
		25%	-	-
3.	[Co(L) <sub>2</sub> (Quino) <sub>2</sub> ]	Stock	17mm	18mm
		75%	16mm	15mm
		50%	-	-
		25%	-	-
4.	[Ni(L <sub>2</sub> ) <sub>2</sub> (en)]	Stock	16mm	16mm
		75%	15mm	15mm
		50%	13mm	14mm
		25%	-	13mm
5.	[Ni(L <sub>2</sub> ) <sub>2</sub> (Py) <sub>2</sub> ]	Stock	15mm	16mm
		75%	14mm	15mm
		50%	-	-
		25%	-	-
6.	[Ni(L <sub>2</sub> ) <sub>2</sub> (Quino) <sub>2</sub> ]	Stock	17mm	15mm
		75%	15mm	12mm
		50%	11mm	-
		25%	-	-
7.	DMSO		-	-



Figure 9: Inhibition Diameter of 2-PhOEtXant Ligand.

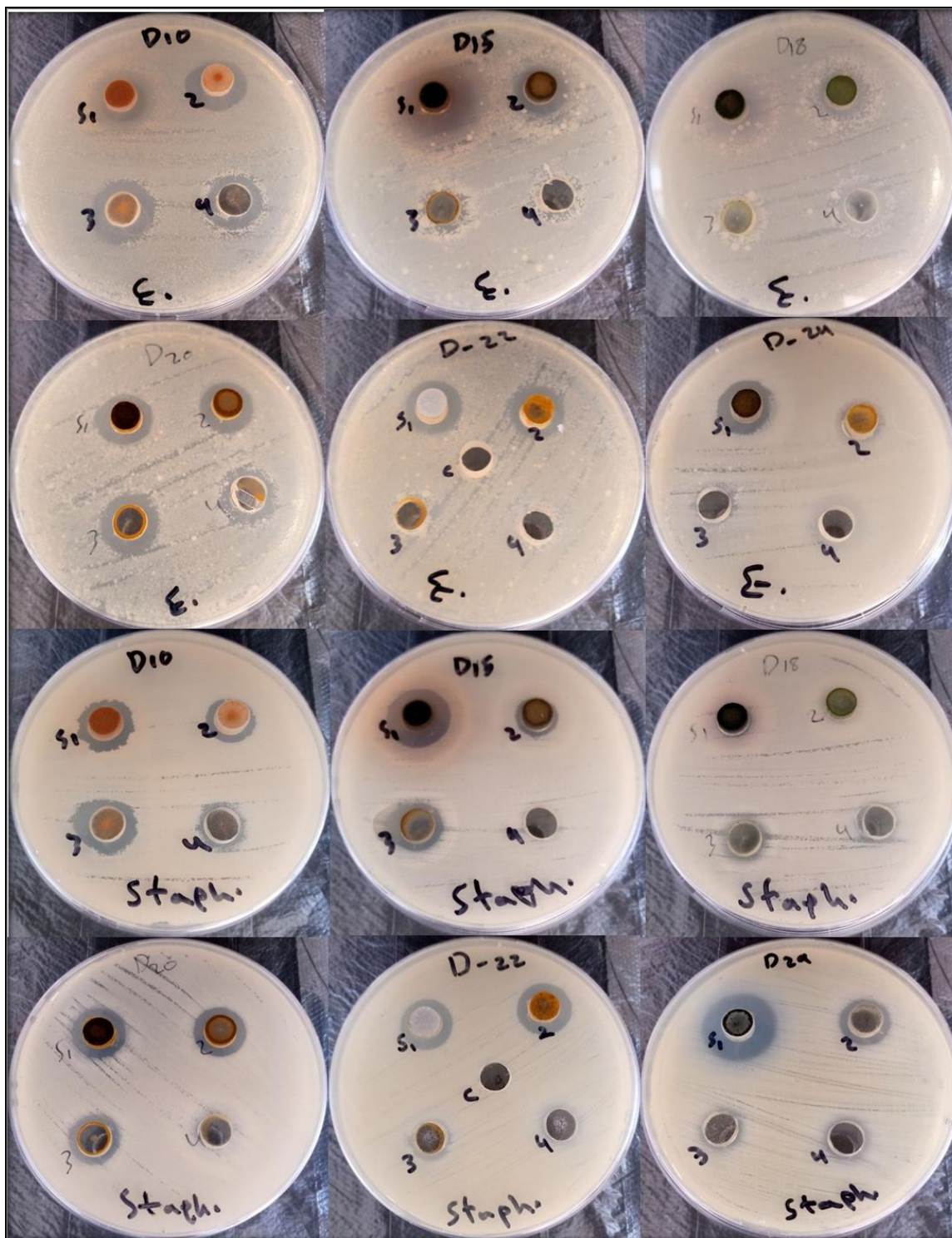
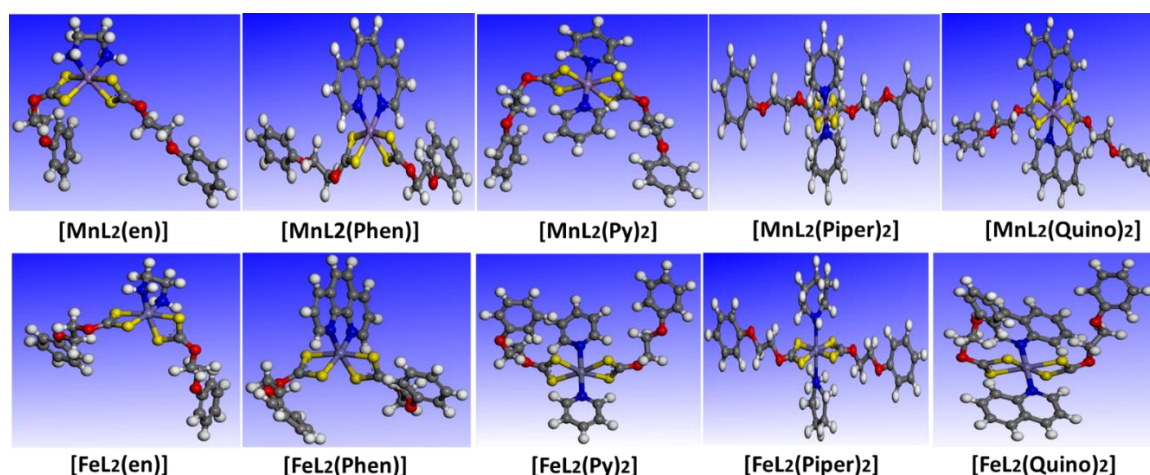
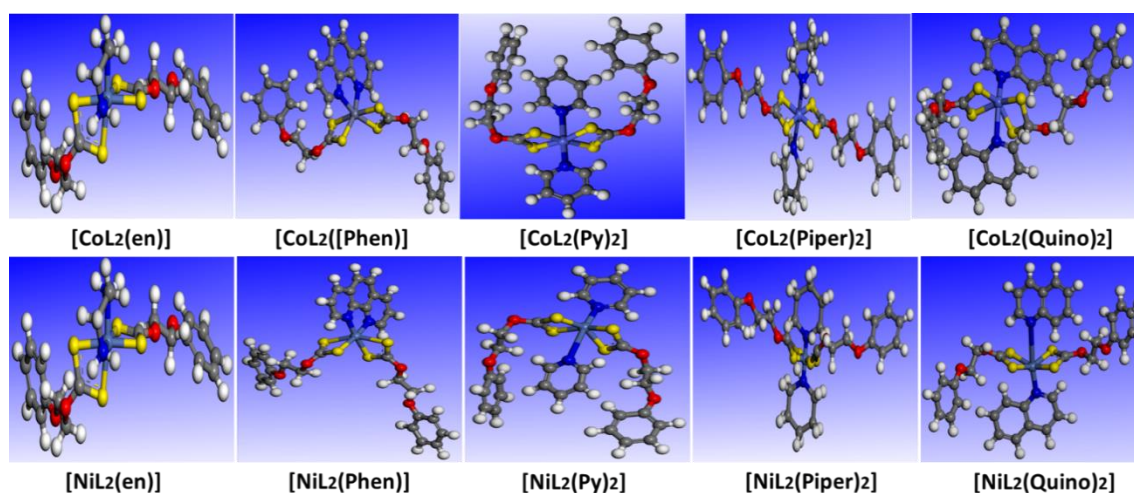


Figure 10: Inhibition Diameter for Complexes Against Bacterial {D10=[Fe(L2)2(Py)2], D15=[Co(L2)2(Phen)], D20=[Ni(L)2(en)], D18=[Co(L)2(Quino)2], D22=[Ni(L2)2(Py)2], D24=[Ni(L2)2(Quino)2]}.

### Theoretical Results

In contemporary times, DFT has emerged as a powerful method for deducing structure, bond angles, bond lengths, thermodynamic parameters, and electronic properties. Our

examination involved the ligand [K(2-MeOEtXant)] and its complexes with both transition and non-transition metals, utilizing DFT computations. The optimized molecular structures, determined by quantum chemical calculations to attain minimum energies, are depicted in (Figs. 11 and 12).

Figure 11: The optimized geometry of Mn<sup>II</sup> & Fe<sup>II</sup> complexes.Figure 12: The optimized geometry of Co<sup>II</sup> & Ni<sup>II</sup> complexes.

## 6. COMPUTATIONAL STUDIES OF THE COMPLEXES

Theoretical computations have indicated that the metal atoms in all complexes display coordination with a distorted octahedral geometry. This geometry is constituted by four sulfur atoms derived from the two chelating 2-phenoxyethyl xanthate ligands and two nitrogen atoms from the nitrogen-based ligands. The calculated bond lengths and bond angles offer valuable insights into the molecular structure of these complexes.

The calculated bond lengths for the metal-sulfur bonds (M-S<sub>1</sub>, M-S<sub>2</sub>, M-S<sub>3</sub>, and M-S<sub>4</sub>) fall within the ranges of [(2.209-2.691), (2.210-2.425), (2.373-2.482) & (2.197- 2.437)], respectively. Similarly, the optimized bond lengths for the metal-

nitrogen bonds (M-N<sub>1</sub>) and (M-N<sub>2</sub>) are found within the ranges of [(1.970-2.517) and (1.966-2.320)], respectively as see in (Table 6). These values align well with the experimental data reported in previous research (Adel, Heja Ibrahim, 2022), (Qadir, 2016) and (Abrahams et al., 1988). The nearly identical bond lengths observed for (C<sub>1</sub>-S<sub>1</sub>) and (C<sub>1</sub>-S<sub>2</sub>), ranging from [(1.669-1.859) and (1.690-1.866)], respectively, suggest the delocalization of (CS<sup>2-</sup>) electrons. Additionally, the optimized bond length for (C<sub>1</sub>-O<sub>1</sub>) falls within the range of (1.328 to 1.540). Furthermore, the bond angles for (S<sub>1</sub>-M-S<sub>4</sub>), (S<sub>2</sub>-M-S<sub>4</sub>), (S<sub>1</sub>-M-S<sub>2</sub>), (S<sub>3</sub>-M-S<sub>4</sub>), and (N<sub>1</sub>-M-N<sub>2</sub>) range from [(79.140-115.992), (84.744-109.872), (72.734-90.000), (73.011-90.000) and (79.474-179.511)], respectively, as calculated using DFT (Table 7).

Table 6: Geometrical bond length for synthesized ligand and their complexes by Dmol3, AGG level.

No.	Compounds	M-S <sub>1</sub>	M-S <sub>2</sub>	M-S <sub>3</sub>	M-S <sub>4</sub>	M-N <sub>1</sub>	M-N <sub>2</sub>	C <sub>1</sub> -S <sub>1</sub>	C <sub>1</sub> -S <sub>2</sub>	C <sub>1</sub> -O <sub>1</sub>
L	[(2-PhOEtXant) K]	---	---	---	---	---	---	1.695	1.695	1.410
1.	[Mn(L) <sub>2</sub> (en)]	2.263	2.281	2.273	2.267	2.023	2.024	1.695	1.700	1.337
2.	[Mn(L) <sub>2</sub> (Phen)]	2.377	2.425	2.374	2.422	2.031	1.988	1.699	1.702	1.348
3.	[Mn(L) <sub>2</sub> (Py) <sub>2</sub> ]	2.280	2.283	2.265	2.242	2.049	2.053	1.711	1.690	1.333
4.	[Mn(L) <sub>2</sub> (Piper) <sub>2</sub> ]	2.398	2.383	2.383	2.395	2.138	2.137	1.808	1.805	1.453
5.	[Mn(L) <sub>2</sub> (Quino) <sub>2</sub> ]	2.270	2.293	2.281	2.254	2.146	2.347	1.690	1.689	1.331
6.	[Fe(L) <sub>2</sub> (en)]	2.254	2.241	2.255	2.244	1.970	1.966	1.694	1.694	1.334
7.	[Fe(L) <sub>2</sub> (Phen)]	2.374	2.372	2.375	2.372	2.208	2.181	1.846	1.845	1.513
8.	[Fe(L) <sub>2</sub> (Py) <sub>2</sub> ]	2.406	3.293	2.405	2.409	2.151	2.149	1.859	1.861	1.511
9.	[Fe(L) <sub>2</sub> (Piper) <sub>2</sub> ]	2.314	2.362	2.358	2.301	2.173	2.165	1.713	1.702	1.354
10.	[Fe(L) <sub>2</sub> (Quino) <sub>2</sub> ]	2.403	2.418	2.416	2.409	2.182	2.174	1.848	1.866	1.515
11.	[Co(L) <sub>2</sub> (en)]	2.373	2.373	2.372	2.370	2.040	2.403	1.847	1.847	1.512
12.	[Co(L) <sub>2</sub> (Phen)]	2.377	2.425	2.374	2.422	2.031	1.988	1.699	1.702	1.348
13.	[Co(L) <sub>2</sub> (Py) <sub>2</sub> ]	2.261	2.210	2.245	2.260	2.403	2.040	1.684	1.697	1.346

14.	[Co(L) <sub>2</sub> (Piper) <sub>2</sub> ]	2.245	2.307	2.259	2.197	2.517	2.005	1.669	1.731	1.339
15.	[Co(L) <sub>2</sub> (Quino) <sub>2</sub> ]	2.209	2.170	2.321	2.306	2.413	1.932	1.854	1.828	1.408
16.	[Ni(L) <sub>2</sub> (en)]	2.375	2.373	2.306	2.395	2.086	2.044	1.688	1.693	1.333
17.	[Ni(L) <sub>2</sub> (Phen)]	2.691	2.416	2.334	2.437	2.003	2.010	1.684	1.691	1.334
18.	[Ni(L) <sub>2</sub> (Py) <sub>2</sub> ]	2.219	2.204	2.195	2.194	2.502	2.000	1.689	1.686	1.328
19.	[Ni(L) <sub>2</sub> (Piper) <sub>2</sub> ]	2.320	2.320	2.320	2.320	2.320	2.320	1.810	1.810	1.540
20.	[Ni(L) <sub>2</sub> (Quino) <sub>2</sub> ]	2.206	2.206	2.215	2.202	2.114	2.771	1.693	1.685	1.329

Table 7: Geometrical bond angle for synthesized complexes by Dmol3, GGA level.

No.	Compounds	S <sub>1</sub> -M-S <sub>4</sub>	S <sub>2</sub> -M-S <sub>3</sub>	S <sub>1</sub> -M-S <sub>2</sub>	S <sub>3</sub> -M-S <sub>4</sub>	N <sub>1</sub> -M-N <sub>2</sub>
1.	[Mn(L) <sub>2</sub> (en)]	104.228	102.349	75.958	75.850	84.334
2.	[Mn(L) <sub>2</sub> (Phen)]	105.248	84.744	72.734	73.011	79.474
3.	[Mn(L) <sub>2</sub> (Py) <sub>2</sub> ]	105.711	101.170	77.226	76.265	179.395
4.	[Mn(L) <sub>2</sub> (Piper) <sub>2</sub> ]	103.335	104.128	76.316	76.335	176.184
5.	[Mn(L) <sub>2</sub> (Quino) <sub>2</sub> ]	103.125	103.855	76.314	76.875	177.626
6.	[Fe(L) <sub>2</sub> (en)]	97.419	97.525	76.867	76.806	85.772
7.	[Fe(L) <sub>2</sub> (Phen)]	101.222	86.744	73.798	73.011	79.474
8.	[Fe(L) <sub>2</sub> (Py) <sub>2</sub> ]	93.701	93.711	81.630	81.631	89.778
9.	[Fe(L) <sub>2</sub> (Piper) <sub>2</sub> ]	99.636	109.872	75.346	75.330	179.466
10.	[Fe(L) <sub>2</sub> (Quino) <sub>2</sub> ]	103.160	105.662	75.380	75.797	179.511
11.	[Co(L) <sub>2</sub> (en)]	93.228	95.349	75.958	75.850	84.334
12.	[Co(L) <sub>2</sub> (Phen)]	89.988	83.290	74.711	74.345	84.350
13.	[Co(L) <sub>2</sub> (Py) <sub>2</sub> ]	104.963	99.653	77.309	77.396	178.508
14.	[Co(L) <sub>2</sub> (Piper) <sub>2</sub> ]	115.992	86.608	62.977	82.791	150.420
15.	[Co(L) <sub>2</sub> (Quino) <sub>2</sub> ]	91.358	96.668	81.133	76.764	161.764
16.	[Ni(L) <sub>2</sub> (en)]	102.062	97.665	75.681	76.141	83.778
17.	[Ni(L) <sub>2</sub> (Phen)]	89.938	83.260	74.700	74.715	81.320
18.	[Ni(L) <sub>2</sub> (Py) <sub>2</sub> ]	79.140	96.455	78.380	78.546	169.939
19.	[Ni(L) <sub>2</sub> (Piper) <sub>2</sub> ]	90.090	90.000	90.000	90.000	180.001
20.	[Ni(L) <sub>2</sub> (Quino) <sub>2</sub> ]	94.925	95.039	78.330	78.106	168.232

### Electronic Properties

To present and discuss our findings, we examined the relaxed state of metal complex molecules, as depicted in (Fig. 5 and 6). These molecules were relaxed using DFT calculations with the Dmol3 method at the GGA (Generalized Gradient Approximation) level, specifically using the PBE (Perdew-Burke-Ernzerhof) exchange-correlation functional. In (Table 7), we have compiled various properties of these metal complexes, such as the energy of the highest occupied molecular orbitals (EHOMO), the energy of the lowest unoccupied molecular orbitals (ELUMO), and the energy gap (E<sub>gap</sub>); and all are measured in electron volts (eV). These properties were determined at the energy minima using DFT calculations with the Dmol3 method at the GGA/PBE level (Alongamo et al., 2022), (Hussein N Najeeb et al., 2020) and (Abdullah et al., 2021).

Our findings indicate that the energy gap required for an electron to transit from the  $\pi \rightarrow \pi^*$  orbital in the complex structure is smaller compared to that of the free ligand. This reduced energy gap signifies a higher likelihood of electron transitions to higher energy states within the metal complex. Consequently, this heightened reactivity and increased polarizability observed

in the metal complex hold promise for future applications in the field of optoelectronics. Frontier orbitals hold significant importance in understanding the chemical characteristics of compounds. Figures 13 to 16 depict the distribution of HOMO (the highest occupied molecular orbital) energy, LUMO (the lowest unoccupied molecular orbital) energy, and the energy gap for the investigated compounds. In these figures, positive charge regions are represented by the color blue, while negative charge regions are indicated in yellow. The eigenvalues of HOMO, LUMO, and their gap energy can provide insights into the biological activity of the molecule. Smaller frontier orbital gaps indicate higher polarizability and are typically associated with greater chemical reactivity and lower kinetic stability (Hussein & Ahmed, 2023) (Hussein Neama Najeeb et al., 2019) and (Juncal et al., 2017).

Table 8 provides further details on various quantum chemical properties, including electron affinity (EA), ionization potential (IP), dipole moment (D), hardness ( $\eta$ ), softness (S), absolute electronegativity ( $\chi$ ), chemical potential ( $\mu$ ), and electrophilicity index ( $\omega$ ). These properties were determined using DFT calculations with the Dmol3 method at the GGA/PBE level and serve to explain the activity of the molecular structures.

Table 8: Electronic parameters, expressed in atomic units (a.u.) with 1 a.u. equivalent to 27.211 electron volts, were computed for the prepared ligand and its complexes using the Dmol3 method at the GGA.

No	E <sub>HOMO</sub>	E <sub>LUMO</sub>	E <sub>gap</sub>	(IP)	(EA)	( $\eta$ )	(S)	( $\chi$ )	( $\mu$ )	( $\omega$ )	(D)
L	-3.988	-2.971	-1.017	3.988	2.971	0.5085	1.9665	-3.4795	3.4795	11.904	11.0430
1.	-3.194	-2.761	-0.433	3.194	2.761	0.2165	4.6189	-2.902	2.902	19.449	7.1105
2.	-3.635	-3.045	-0.590	3.635	3.045	0.2950	3.3898	-3.340	3.340	18.907	4.2432

3.	- 3.79 2	-3.469	-0.323	3.792	3.469	0.1615	6.1919	-3.630	3.630	40.806	1.5325
4.	- 3.26 9	-3.071	-0.098	3.269	3.071	0.0490	20.408	-3.170	3.170	102.53	4.7217
5.	- 3.50 3	-3.405	-0.098	3.503	3.071	0.0490	20.408	-3.454	3.454	121.73	0.7978
6.	- 3.30 2	-2.023	-1.279	3.302	2.023	0.6395	1.5637	-2.662	2.662	5.5425	6.2315
7.	- 4.41 4	-3.879	-0.535	4.414	3.879	0.2675	3.7383	-4.146	4.146	17.193	
8.	- 3.83 5	-3.460	-0.375	3.835	3.460	0.1875	5.3333	-7.295	7.295	53.217	
9.	- 2.78 5	-1.903	-0.882	2.785	1.903	0.4410	2.2675	-4.688	4.688	21.977	0.7653
10.	- 4.51 1	-3.870	-0.641	4.511	3.870	0.3205	3.1201	-4.190	4.190	27.395	3.2871
11.	- 4.35 4	-3.795	0.559	4.354	3.795	0.2795	3.5778	-4.074	4.074	16.601	
12.	- 4.23 4	-3.786	-0.448	4.234	3.786	0.2240	4.4642	-4.010	4.010	35.893	
13.	- 3.40 5	-2.705	-0.700	3.405	2.705	0.3500	2.8571	-3.055	3.055	13.332	1.8762
14.	- 2.82 4	-2.153	-0.671	2.824	2.153	0.3355	2.9806	-2.488	2.488	9.2289	0.3641
15.	- 4.56 3	-3.916	-0.647	4.563	3.916	0.3235	3.0911	-4.239	4.239	27.779	3.0753
16.	- 3.28 2	-2.837	-0.445	3.282	2.837	0.2225	4.4943	-3.059	3.059	21.034	5.7759
17.	- 3.41 8	-3.250	-0.168	3.418	3.250	0.0840	11.904	-3.334	3.334	66.164	7.5825
18.	- 4.07 3	-2.981	-1.092	4.073	2.981	0.5460	1.8315	-3.527	3.527	11.391	1.7787
19.	- 3.41 7	-3.245	-0.172	3.417	3.245	0.0860	11.627	-3.331	3.331	64.509	5.0210
20.	- 4.09 4	-3.048	-1.046	4.094	3.048	0.5230	1.9120	-3.571	3.571	12.191	1.6902

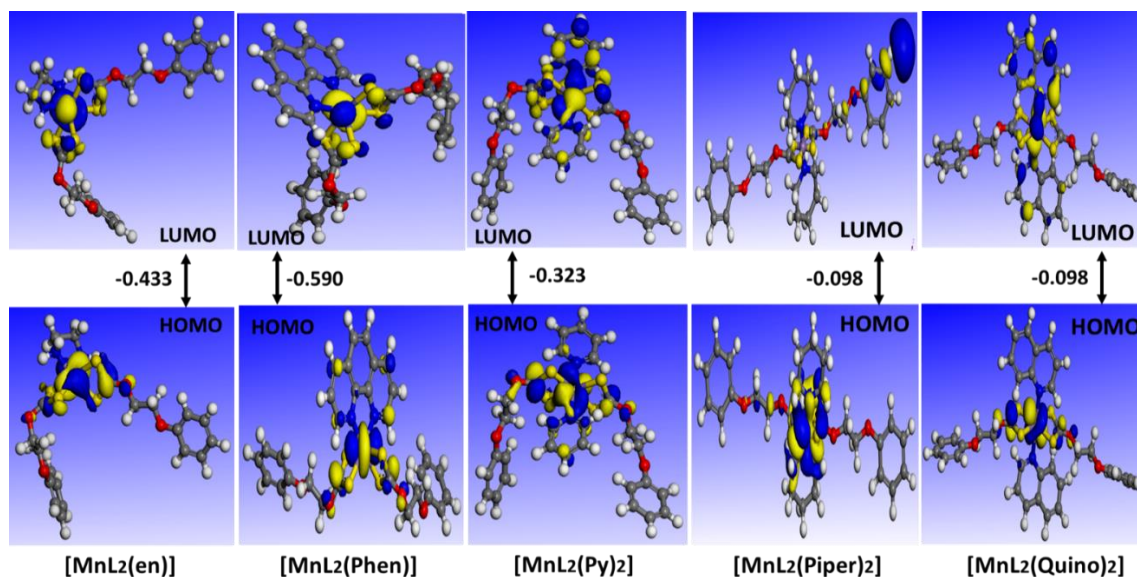


Figure 13: The HOMO, LUMO & Egap of the Mn<sup>II</sup> complexes.

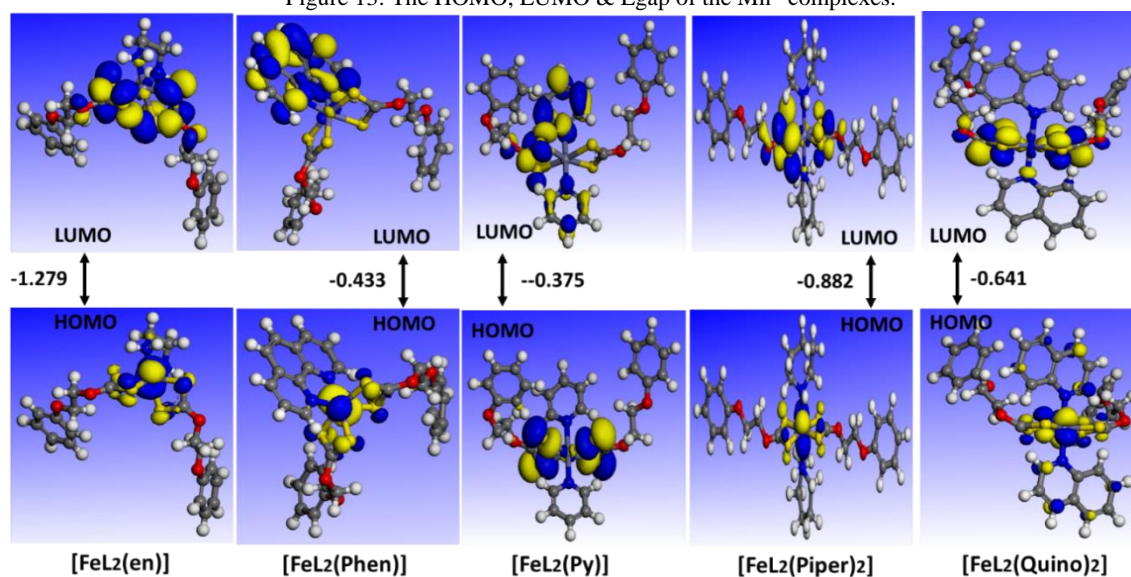


Figure 14: The HOMO, LUMO & Egap of the Fe<sup>II</sup> complexes.

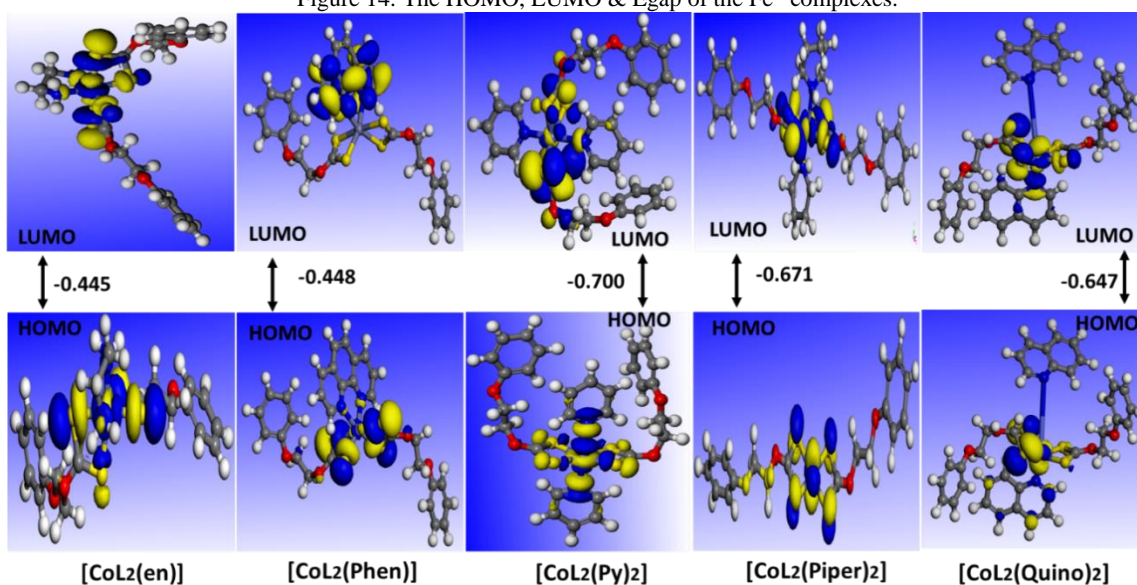
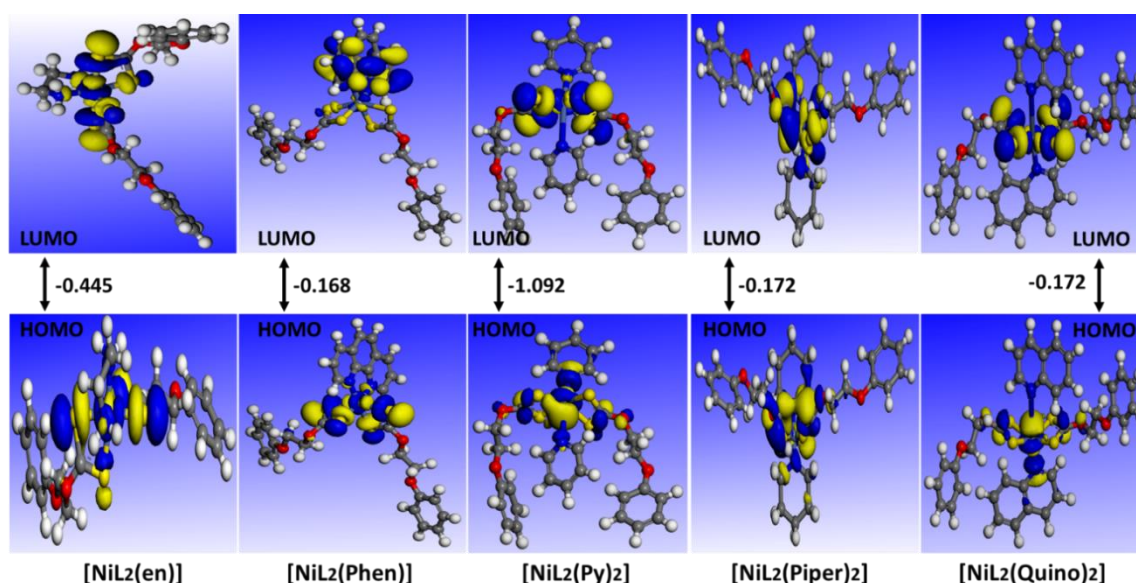


Figure 15: The HOMO, LUMO & Egap of the Co<sup>II</sup> complexes.

Figure 16: The HOMO, LUMO & Egap of the Ni<sup>II</sup> complexes.

### Thermodynamic Parameters

To establish a comprehensive understanding of the relationships between the energetic, structural, and reactivity characteristics of dithiocarbonate complexes, we conducted quantum-mechanical calculations to ascertain various thermodynamic parameters. These parameters include significant values like zero-point vibrational energy, entropy, enthalpy, internal energy, and specific heat capacity for both the ligands

and the corresponding complexes (Jassim et al., 2021), (Mensah et al., 2021) and (Mohamed et al., 2004). Our calculations were performed utilizing the DFT method with the Dmol3 approach at the GGA/PBE level. These calculations were conducted under standard conditions, specifically at a temperature of 298.15 K and a pressure of 1 atm. The resulting values obtained from these calculations have been documented in (Table 9) for reference and analysis.

Table 9: presents the computed thermodynamic parameters for all complexes alongside the ligand, offering insights into their thermodynamic stability and characteristics.

No.	Compounds	Binding Energy (kcal/mol)	Total Energy (kcal/mol)	Zero-point vibrational energies (kcal/mol)	Gibbs free energy (kcal/mol)	Enthalpy (kcal/mol)	Entropy (calmol <sup>-1</sup> K <sup>-1</sup> )	Specific heat Cv (calmol <sup>-1</sup> K <sup>-1</sup> )
L	[(2-MeOEtXant)K]	-2368.257	-		64.489	101.071	122.695	57.645
1.	[Mn(L) <sub>2</sub> (en)]	-6866.806	-	274.436	229.778	295.138	219.219	122.174
2.	[Mn(L) <sub>2</sub> (Phen)]	-7875.244	-	312.094	273.077	331.712	196.663	128.222
3.	[Mn(L) <sub>2</sub> (Py) <sub>2</sub> ]	-8533.044	-	314.486	270.790	336.856	221.584	137.784
4.	[Mn(L) <sub>2</sub> (Piper) <sub>2</sub> ]	-371.694	2656349.29	397.503	362.201	414.889	176.716	116.708
5.	[Mn(L) <sub>2</sub> (Quino) <sub>2</sub> ]	-10358.37	-	371.613	321.179	398.310	258.696	164.071
6.	[Fe(L) <sub>2</sub> (en)]	-6909.157	-	274.567	234.585	293.952	199.120	117.888
7.	[Fe(L) <sub>2</sub> (Phen)]	-8444.481	-	244.989	256.074	298.057	211.248	163.987
8.	[Fe(L) <sub>2</sub> (Py) <sub>2</sub> ]	-8338.519	-	312.684	269.188	335.276	221.659	138.0.23
9.	[Fe(L) <sub>2</sub> (Piper) <sub>2</sub> ]	-8396.307	-	401.280	353.858	425.447	240.110	145.954
10.	[Fe(L) <sub>2</sub> (Quino) <sub>2</sub> ]	-8835.159	-	333.669	293.543	359.907	222.587	182.175
11.	[Co(L) <sub>2</sub> (en)]	-7809.157	-	374.567	334.665	293.952	211.129	117.888
12.	[Co(L) <sub>2</sub> (Phen)]	-9891.932	-	412.094	343.077	431.712	196.663	168.222
13.	[Co(L) <sub>2</sub> (Py) <sub>2</sub> ]	-8578.519	-	312.684	269.188	335.276	221.659	138.0.23
14.	[Co(L) <sub>2</sub> (Piper) <sub>2</sub> ]	-8391.530	-	400.138	361.109	420.438	198.992	130.234

15.	[Co(L) <sub>2</sub> (Quino) <sub>2</sub> ]	-9406.621	- 2998181.15	375.995	326.191	402.047	254.423	162.210
16.	[Ni(L) <sub>2</sub> (en)]	-6898.745	- 2680538.08	271.904	230.266	292.272	207.971	120.030
17.	[Ni(L) <sub>2</sub> (Phen)]	-8861.932	- 2917615.11	244.989	256.074	298.057	211.248	163.987
18.	[Ni(L) <sub>2</sub> (Py) <sub>2</sub> ]	-8575.330	- 2870906.34	311.545	261.784	335.358	246.767	140.168
19.	[Ni(L) <sub>2</sub> (Piper) <sub>2</sub> ]	-5286.633	- 2871221.37	376.628	342.055	394.575	176.150	121.906
20.	[Ni(L) <sub>2</sub> (Quino) <sub>2</sub> ]	-10428.43	- 3062051.74	369.395	321.109	395.175	248.416	160.081

## CONCLUSION

The research presented focuses on the synthesis and characterization of dithiolate transition metal complexes, particularly xanthates, with potential applications in various fields. The study explores the coordination chemistry of these complexes, detailing their synthesis processes and comprehensive physical characterization using various analytical techniques.

Key findings include the successful synthesis of potassium 2-phenoxyethyl xanthate ligand and its metal complexes with different transition metal ions. The compounds were thoroughly characterized through techniques such as NMR, FT-IR, magnetic susceptibility measurements, ultraviolet-visible spectroscopy, and thermal analysis.

The results indicate promising biological activities exhibited by the complexes, including notable antioxidant and antibacterial effects. Specifically, the most potent complex demonstrated an IC<sub>50</sub> value of 19.10 against the antioxidant DPPH, suggesting its strong antioxidative properties compared to the other compounds synthesized. Furthermore, our findings reveal that the complexes [Co(L)<sub>2</sub>(Phen)] and [Fe(L)<sub>2</sub>(Py)<sub>2</sub>] exhibit enhanced antibacterial activity relative to the other complexes tested. These observations underscore the potential therapeutic applications of these compounds.

Computational studies using DFT provide insights into the molecular structures, bond lengths, and electronic properties of the complexes. The calculated bond lengths and angles align well with experimental data, supporting the reliability of the computational approach. Electronic properties, frontier orbitals, and thermodynamic parameters further contribute to understanding the reactivity and stability of the synthesized complexes.

The research also emphasizes the potential applications of these complexes in optoelectronics and highlights their promising antioxidant and antibacterial activities. The detailed characterization and computational insights presented in the study contribute to advancing the understanding of dithiolate transition metal complexes, paving the way for further exploration of their applications in various scientific and technological domains.

## REFERENCES

- Abdullah, N. H. S., Ozair, L. N., Anas, M. M. A. M., & Yamin, B. M. (2021). Structural and Electronic Study of Palladium (II) Complexes by a Theoretical Approach. *Journal of Physics: Conference Series*, 1893(1), 12004.
- Abrahams, B. F., Hoskins, B. F., Tiekink, E. R. T., & Winter, G. (1988). Investigation of a new xanthate ligand. The crystal and molecular structures of nickel and cadmium (methoxyethyl) xanthates. *Australian Journal of Chemistry*, 41(7), 1117–1122.
- Adel, Heja Ibrahim, S. E. A. (2022). Synthesis and Characterization of Sulfur Donor Ligand (Xanthate) Complexes with Manganese (II), Iron (II), Cobalt (II), Nickel (II), Copper (II), and Zinc (II) and Their Adduct With Nitrogen Base Ligand. *Journal of Duhok University*, 25(2), 244–260.
- Ajiboye, T. O., & Onwudiwe, D. C. (2022). Synthesis and Antioxidant Investigation of Ag<sub>2</sub>S Nanoparticles Obtained from Silver (I) Complex of N-Methyl-N-Phenyl-Dithiocarbamate. *Journal of Nano Research*, 76, 131–143.
- Al-fahdawi, A., & Alsalihi, E. (2018). Synthesis and Characterization of Iron II, Cobalt II, Nickel II, Copper II, and Zinc II Complexes Using Diphenylmethyl Xanthate Ligand. *Synthesis and Characterization of IronII, CobaltII, NickelIII, CopperII, and ZincII Complexes Using Diphenylmethyl Xan. ARO-The Scientific Journal of Koya University*, 1. <https://doi.org/10.14500/aro.10243>
- Al-Fahdawi, A., & Alsalihi, E. (2018). Synthesis and Characterization of Iron (II), Cobalt (II), Nickel (II), Copper (II), and Zinc (II) Complexes Using Diphenylmethyl Xanthate Ligand. *Aro-The Scientific Journal of Koya University*, 6(1), 33–37.
- Al-Garah, F. K. (2017). Preparation and characterization of some Transition Metal Complexes the first and second with (1-methyl-3-Piperidine Xanthate potassium) and ethylenediamine. *Tikrit Journal of Pure Science*, 22(12), 72–78.
- AL-Mukhtar, S. E., & AL-Jarah, F. K. (2019). Preparation and Characterization of some Transition Metal Complexes with OleylXanthate and 1, 10-Phenanthroline. *Rafidain Journal of Science*, 28(2E: Chem.), 228–234.
- Al Zoubi, W., Karabet, F., Al Bandakji, R., & Hussein, K. (2017). Experimental and theoretical investigations of the antioxidant activity of 2, 2'-methylenebis (4, 6-dialkylphenol) compounds. *Applied Organometallic Chemistry*, 31(2), e3562.
- Alongamo, C. I. L., Tasheh, S. N., Nkungli, N. K., Bine, F. K., & Ghogomu, J. N. (2022). Structural, electronic, and charge transport properties of new materials based on 2-(5-mercapto-1, 3, 4-oxadiazol-2-yl) phenol for organic solar cells and light emitting diodes by DFT and TD-DFT. *Journal of Chemistry*, 2022, p 15.
- Andotra, S., Kalgotra, N., & Pandey, S. K. (2014). Syntheses, Characterization, Thermal, and Antimicrobial Studies of Lanthanum (III) Tollyl/Benzylidithiocarbonates. *Bioinorganic Chemistry and Applications*, 2014.
- Andotra, S., Kumar, S., Kour, M., Sharma, V., Jaglan, S., & Pandey, S. K. (2017). Synthesis, spectroscopic, DFT and in vitro biological studies of vanadium (III) complexes of aryldithiocarbonates. *Spectrochimica Acta Part A: Molecular and Biomolecular Spectroscopy*, 180, 127–137.
- Batten, S. R., & Robson, R. (1998). Interpenetrating nets: ordered, periodic entanglement. *Angewandte Chemie International Edition*, 37(11), 1460–1494.
- Becke, A. (n.d.). Density-functional thermochemistry. III. The

- role of exact exchange (1993) *J. Chem. Phys.*, 98, 5648.
- Cordova, B. M., Infantas, G. C., Mayta, S., Huamani-Palomino, R. G., Kock, F. V. C., de Oca, J. M., & Valderrama, A. C. (2021). Xanthate-modified alginates for the removal of Pb (II) and Ni (II) from aqueous solutions: A brief analysis of alginate xanthation. *International Journal of Biological Macromolecules*, 179, 557–566.
- DHAKA, S., & Choudhary, P. (2015). Synthesis and antibacterial activity of Schiff Base Complexes of Si (IV). *Global Journal of Chemistry*, 1(1), 28–32.
- Faroughi Niya, H., Hazeri, N., & Fatahpour, M. (2021). Synthesis, characterization, and application of CoFe<sub>2</sub>O<sub>4</sub>@ amino-2-naphthol-4-sulfonic acid as a novel and reusable catalyst for the synthesis of spirochromene derivatives. *Applied Organometallic Chemistry*, 35(3), e6119.
- Gaikwad, V. V., Mane, P. A., Dey, S., Patel, D., & Bhanage, B. M. (2020). Supramolecular Pd (II) complex of DPPF and dithiolate: An efficient catalyst for amino and phenoxycarbonylation using Co<sub>2</sub> (CO)<sub>8</sub> as sustainable C1 source. *Molecular Catalysis*, 482, 110672.
- Griffith, D. M., Szócs, B., Keogh, T., Suponitsky, K. Y., Farkas, E., Buglyó, P., & Marmion, C. J. (2011). Suberoylanilide hydroxamic acid, a potent histone deacetylase inhibitor; its X-ray crystal structure and solid state and solution studies of its Zn (II), Ni (II), Cu (II) and Fe (III) complexes. *Journal of Inorganic Biochemistry*, 105(6), 763–769.
- Heimbach, I., Petrus, H. T. B. M., Prasetya, A., Idrus, A., Timotius, D., Kusumastuti, Y., & Sutijan, S. (2023). Studi Recovery Tembaga pada Proses Froth Flotation dari Bijih Tembaga Papua, Indonesia dengan Variasi pH dan Konsentrasi Kolektor. *Seminar Nasional Teknik Kimia "Kejuangan"*, 1–8.
- Hussein, S. Z., & Ahmed, H. (2023). Design, structural and electronic properties of PVA/SeO<sub>2</sub> structure: DFT study. *AIP Conference Proceedings*, 2591(1), p 40036.
- Jassim, S., Abbas, A., AL-Shakban, M., & Ahmed, L. (2021). Chemical Vapour Deposition of CdS Thin Films at Low Temperatures from Cadmium Ethyl Xanthate. *Egyptian Journal of Chemistry*, 64(5), 2533–2538.
- Juncal, L. C., Avila, J., Asensio, M. C., Della Védova, C. O., & Romano, R. M. (2017). Electronic structure determination using an assembly of conventional and synchrotron techniques: The case of a xanthate complex. *Spectrochimica Acta Part A: Molecular and Biomolecular Spectroscopy*, 180, 183–192.
- Khoo, T.-J., bin Break, M. K., Crouse, K. A., Tahir, M. I. M., Ali, A. M., Cowley, A. R., Watkin, D. J., & Tarafder, M. T. H. (2014). Synthesis, characterization and biological activity of two Schiff base ligands and their nickel (II), copper (II), zinc (II) and cadmium (II) complexes derived from S-4-picolylidithiocarbamate and X-ray crystal structure of cadmium (II) complex derived fro. *Inorganica Chimica Acta*, 413, 68–76.
- Lee, C., Yang, W., & Parr, R. G. (1988). Development of the Colle-Salvetti correlation-energy formula into a functional of the electron density. *Physical Review B*, 37(2), 785.
- Mane, P. A., Dey, S., & Vivekananda, K. V. (2017). Macrocyclic Pd (II) dithiolate complexes as catalysts in Heck reactions. *Tetrahedron Letters*, 58(1), 25–29.
- Martell, A. E. (1971). Coordination chemistry van Nostrand Reinhold. *New York*, 1, 55–56.
- McNaughten, P. D., Saah, S. A., Akhtar, M., Abdulwahab, K., Malik, M. A., Raftery, J., Awudza, J. A. M., & O'Brien, P. (2016). The effect of alkyl chain length on the structure of lead (II) xanthates and their decomposition to PbS in melt reactions. *Dalton Transactions*, 45(41), 16345–16353.
- Mensah, M. B., Awudza, J. A. M., Revaprasadu, N., & O'Brien, P. (2021). Synthesis of CdS and PbS nanoparticles by the thermal decomposition of ethyl xanthate complexes in castor oil using the heat-up technique. *Materials Science in Semiconductor Processing*, 122, 105493.
- Mikheyli, A. V., Grivin, V. P., & Plyusnin, V. F. (2023). Spectroscopy and kinetics of intermediates in photochemistry of xanthate Ni (S<sub>2</sub>COEt)<sub>2</sub> complex in CCl<sub>4</sub>. *Journal of Photochemistry and Photobiology A: Chemistry*, 435, 114260.
- Mohamed, A. A., Kani, I., Ramirez, A. O., & Fackler, J. P. (2004). Synthesis, characterization, and luminescent properties of dinuclear gold (I) xanthate complexes: X-ray structure of [Au<sub>2</sub> (n Bu-xanthate)<sub>2</sub>]. *Inorganic Chemistry*, 43(13), 3833–3839.
- Montagner, D., Marzano, C., & Gandin, V. (2011). Synthesis, characterization and cytotoxic activity of palladium (II) dithiocarbamate complexes with  $\alpha$ ,  $\omega$ -diamines. *Inorganica Chimica Acta*, 376(1), 574–580.
- Najeeb, Hussein N, Abed, M. K., & Hussein, S. A. (2020). Quantum Chemical Studies on the Molecular Structure and Electronic Properties of Tin-Metal Complexes. *TEST ENGINEERING AND MANAGEMENT*, 83(5–6), 12881–12887.
- Najeeb, Hussein Neama, Ammer ALshareefi, M. A., & Abbood, H. I. (2019). Quantum Chemical Studies on the Molecular Structure and Electronic Properties of Rhenium Metal Complexes. *Indian Journal of Forensic Medicine & Toxicology*, 13(4), p 924.
- Nicholls, D. (2013). *The chemistry of iron, cobalt and nickel: comprehensive inorganic chemistry* (Vol. 24). Elsevier.
- Palaty, S., Devi, P. V., & Mary, K. J. (2010). Characterisation and thermal decomposition behaviour of xanthate compounds. *Progress in Rubber Plastics and Recycling Technology*, 26(4), 199–214.
- Parcheta, M., Świsłocka, R., Orzechowska, S., Akimowicz, M., Chojińska, R., & Lewandowski, W. (2021). Recent developments in effective antioxidants: The structure and antioxidant properties. *Materials*, 14(8), 1984.
- Peyrat-Maillard, M. N., Bonnely, S., & Berset, C. (2000). Determination of the antioxidant activity of phenolic compounds by coulometric detection. *Talanta*, 51(4), 709–716.
- Plyusnin, V. F., Mikheyli, A. V., Grivin, V. P., & Shubin, A. A. (2021). Photochemistry of Dithiocarbamate Ni (S<sub>2</sub>P (i-Bu)<sub>2</sub>)<sub>2</sub> Complexes in CCl<sub>4</sub>. Transient Species and TD-DFT Calculations. *XXVIII Международная Чугаевская Конференция По Координационной Химии*, p 111-111.
- Qadir, A. M. (2016). Synthesis and Crystal Structure of o-Methoxyethylidithiocarbonato Nickel (II) Complex involving Tetramethylethylenediamine. *Asian Journal of Chemistry*, 28(5), 1169.
- Rajput, G., Singh, V., Singh, S. K., Prasad, L. B., Drew, M. G. B., & Singh, N. (2012). Cooperative Metal-Ligand-Induced Properties of Heteroleptic Copper (I) Xanthate/Dithiocarbamate PPh<sub>3</sub> Complexes. *European Journal of Inorganic Chemistry*, 2012(24), 3885–3891.
- Rathore, H., Varshney, G., Mojumdar, S., & Saleh, M. (2007). Synthesis, characterization and fungicidal activity of zinc diethylidithiocarbamate and phosphate. *Journal of Thermal Analysis and Calorimetry*, 90(3), 681–686.
- Shahzadi, S., Ali, S., Jabeen, R., & KHOSA, M. K. (2009). [Pd (Me-Xanthate)<sub>2</sub>]: Synthesis, Characterization, and X-Ray Structure. *Turkish Journal of Chemistry*, 33(2), 307–312.
- Siddiqi, K. S., & Nishat, N. (2000). Synthesis and characterization of succinimide and phthalohydro dithiocarbamates and their complexes with some transition metal ions. *Synthesis and Reactivity in Inorganic and Metal-Organic Chemistry*, 30(8), 1505–

- 1518.
- Singh, N., Singh, N. K., & Kaw, C. (1989). Synthetic and spectroscopic studies of xanthato-bridged heterobimetallic complexes containing diamagnetic and paramagnetic metal ions. *Bulletin of the Chemical Society of Japan*, 62(10), 3328–3333.
- Solovyev, A. I., Mikheyli, A. V., Plyusnin, V. F., Shubin, A. A., Grivin, V. P., Larionov, S. V., Tkachenko, N. V., & Lemmetyinen, H. (2019). Photochemistry of dithiophosphinate Ni (S2P (i-Bu) 2) 2 complex in CCl4. Transient species and TD-DFT calculations. *Journal of Photochemistry and Photobiology A: Chemistry*, 381, 111857.
- Sreeju, N., Rufus, A., & Philip, D. (2016). Microwave-assisted rapid synthesis of copper nanoparticles with exceptional stability and their multifaceted applications. *Journal of Molecular Liquids*, 221, 1008–1021.
- Vakalopoulou, E., Buchmaier, C., Pein, A., Saf, R., Fischer, R. C., Torvisco, A., Warchomicka, F., Rath, T., & Trimmel, G. (2020). Synthesis and characterization of zinc di (O-2, 2-dimethylpentan-3-yl dithiocarbonates) bearing pyridine or tetramethylethylenediamine coligands and investigation of their thermal conversion mechanisms towards nanocrystalline zinc sulfide. *Dalton Transactions*, 49(41), 14564–14575.